

This is a repository copy of Synthetic protein binders reveal a cryptic regulatory pocket on Aurora A for selective allosteric inhibition.

White Rose Research Online URL for this paper: https://eprints.whiterose.ac.uk/id/eprint/233086/

Version: Preprint

Preprint:

Roberts*, J.P., Holder*, J. orcid.org/0000-0001-7597-3104, Shami-Inkindi, G.B. et al. (12 more authors) (2025) Synthetic protein binders reveal a cryptic regulatory pocket on Aurora A for selective allosteric inhibition. [Preprint - Research Square]

https://doi.org/10.21203/rs.3.rs-7565154/v1

Reuse

This article is distributed under the terms of the Creative Commons Attribution (CC BY) licence. This licence allows you to distribute, remix, tweak, and build upon the work, even commercially, as long as you credit the authors for the original work. More information and the full terms of the licence here: https://creativecommons.org/licenses/

Takedown

If you consider content in White Rose Research Online to be in breach of UK law, please notify us by emailing eprints@whiterose.ac.uk including the URL of the record and the reason for the withdrawal request.





Synthetic protein binders reveal a cryptic regulatory pocket on Aurora A for selective allosteric inhibition

Jack P. Roberts*

Division of Molecular Medicine, Leeds Institute of Medical Research, University of Leeds, Leeds LS9 7TF, UK; School of Molecular and Cellular Biology, University of Leeds, Leeds LS2 9JT, UK; Astbury Centre for Structural and Molecular Biology, University of Leeds, Leeds LS2 9JT, UK

James Holder*

Department of Biochemistry, University of Oxford, S Parks Rd, Oxford OX1 3QU https://orcid.org/0000-0001-7597-3104

Gamaliel B. Shami-Inkindi

School of Molecular and Cellular Biology, University of Leeds, Leeds LS2 9JT, UK; Astbury Centre for Structural and Molecular Biology, University of Leeds, Leeds LS2 9JT, UK

Isha A. Mohan

School of Molecular and Cellular Biology, University of Leeds, Leeds LS2 9JT, UK; Astbury Centre for Structural and Molecular Biology, University of Leeds, Leeds LS2 9JT, UK https://orcid.org/0009-0006-2561-0851

Paul A. Cordell

School of Molecular and Cellular Biology, University of Leeds, Leeds LS2 9JT, UK; Astbury Centre for Structural and Molecular Biology, University of Leeds, Leeds LS2 9JT, UK

Jennifer A. Miles

School of Molecular and Cellular Biology, University of Leeds, Leeds LS2 9JT, UK; Astbury Centre for Structural and Molecular Biology, University of Leeds, Leeds LS2 9JT, UK

Faye Blinkhome

School of Molecular and Cellular Biology, University of Leeds, Leeds LS2 9JT, UK; Astbury Centre for Structural and Molecular Biology, University of Leeds, Leeds LS2 9JT, UK

Christian Tiede

School of Molecular and Cellular Biology, University of Leeds, Leeds LS2 9JT, UK; Astbury Centre for Structural and Molecular Biology, University of Leeds, Leeds LS2 9JT, UK https://orcid.org/0000-0003-0280-4005

Mark W. Richards

School of Molecular and Cellular Biology, University of Leeds, Leeds LS2 9JT, UK; Astbury Centre for Structural and Molecular Biology, University of Leeds, Leeds LS2 9JT, UK https://orcid.org/0000-0003-1108-2825

Thembaninkosi G. Gaule

Astbury Centre for Structural and Molecular Biology, University of Leeds, Leeds LS2 9JT, UK; Leeds Institute of Cardiovascular and Metabolic Medicine, School of Medicine, University of Leeds, Leeds, LS2 9JT, UK

Claire E. L. Smith

Division of Molecular Medicine, Leeds Institute of Medical Research, University of Leeds, Leeds LS9 7TF, UK; School of Dentistry, University of Leeds, Leeds, LS9 7TF https://orcid.org/0000-0001-8320-5105

Fanni Gergely

Department of Biochemistry, University of Oxford, S Parks Rd, Oxford OX1 3QU https://orcid.org/0000-0002-2441-8095

Richard Bayliss

School of Molecular and Cellular Biology, University of Leeds, Leeds LS2 9JT, UK; Astbury Centre for Structural and Molecular Biology, University of Leeds, Leeds LS2 9JT, UK https://orcid.org/0000-0003-0604-2773

Colin A. Johnson

C.Johnson@leeds.ac.uk

Division of Molecular Medicine, Leeds Institute of Medical Research, University of Leeds, Leeds LS9 7TF, UK

Darren Tomlinson

d.c.tomlinson@leeds.ac.uk

School of Molecular and Cellular Biology, University of Leeds, Leeds LS2 9JT, UK; Astbury Centre for Structural and Molecular Biology, University of Leeds, Leeds LS2 9JT, UK https://orcid.org/0000-0003-4134-7484

Article

Keywords:

Posted Date: October 3rd, 2025

DOI: https://doi.org/10.21203/rs.3.rs-7565154/v1

License: © ① This work is licensed under a Creative Commons Attribution 4.0 International License. Read Full License

Additional Declarations: There is **NO** Competing Interest.

Synthetic protein binders reveal a cryptic regulatory pocket on Aurora A for selective allosteric inhibition

Jack P Roberts^{1,2,3*}, James Holder^{4*}, Gamaliel B Shami-Inkindi^{2,3}, Isha A Mohan^{2,3}, Paul A Cordell^{2,3}, Jennifer A Miles^{2,3}, Faye Blinkhorne^{2,3}, Christian Tiede^{2,3}, Mark W Richards^{2,3}, Thembaninkosi G Gaule^{3,5}, Claire E L Smith^{1,6}, Fanni Gergely⁴, Richard Bayliss^{2,3}, Colin A Johnson¹ and Darren C Tomlinson^{2,3}.

¹Division of Molecular Medicine, Leeds Institute of Medical Research, University of Leeds, Leeds LS9 7TF, UK | ²School of Molecular and Cellular Biology, University of Leeds, Leeds LS2 9JT, UK | ³Astbury Centre for Structural and Molecular Biology, University of Leeds, Leeds LS2 9JT, UK | ⁴Department of Biochemistry, University of Coxford, S Parks Rd, Oxford OX1 3QU | ⁵Leeds Institute of Cardiovascular and Metabolic Medicine, School of Medicine, University of Leeds, Leeds, LS2 9JT, UK | ⁶School of Dentistry, University of Leeds, Leeds, LS2 7TF |

*Indicates authors contributed equally to this work

Colin A Johnson: C.Johnson@leeds.ac.uk Darren Tomlinson: D.C.Tomlinson@leeds.ac.uk

Abstract:

Aurora Kinase A (AurA) is an essential mitotic kinase and therapeutic target in cancer. Most protein kinase inhibitors target the conserved ATP-binding pocket, often resulting in poor selectivity and off-target effects. Here, we identify and characterise small synthetic protein binders, Adhirons, as allosteric inhibitors of AurA. Using 'phage display, we isolated Adhiron reagents that bind a previously uncharacterised site on the αG-helix of the kinase C-lobe. Structural and biochemical analyses revealed that the Adhiron inhibited AurA by modulating the activation loop via this cryptic site, which we designate the **T-pocket**. In cells, Adhiron expression mimics the effects of small molecule inhibitors of AurA on substrate and autophosphorylation, while sparing Aurora kinase B and without impairing TPX2-mediated localisation of AurA to the mitotic spindle. The AurA-inhibitory Adhirons demonstrate remarkable selectivity, potency and affinity, a highly sought-after combination of properties for kinase inhibition facilitating their use as tractable research tools for probing AurA function and as pharmacophore templates for structure-based drug design. Finally, these reagents illustrate a generalisable strategy for targeting allosteric sites across the Kinome.

Introduction:

Serine/threonine kinases are an abundant class of proteins which phosphorylate specific serine or threonine residues. Increased activity of many kinases is associated with cancer onset and progression, making protein kinases the second largest group of drug targets after G-protein-coupled receptors [1]. In general, kinase inhibitors target highly conserved, structurally similar ATP-binding sites, often producing off-target effects [2, 3]. Allosteric inhibitor development may circumvent these issues by targeting less conserved sites [4], but identifying suitable and druggable allosteric sites is difficult.

The Aurora family of serine/threonine kinases consists of three members: Aurora A (AurA), Aurora B (AurB), and Aurora C (AurC), which all contain a highly conserved catalytic domain. Although sharing high sequence similarity, they differ in their localisation and functions. Both AurA and AurB have essential roles in regulating cell division during mitosis, whereas AurC has a unique role during spermatogenesis [5, 6]. AurA is a promiscuous protein with several known interactors, notably CEP192, N-Myc, TACC3 and TPX2 [7-10]. Structurally, AurA adopts a canonical kinase fold, an ATP binding pocket hinged between a largely but not exclusively β-sheet N-terminal lobe (N-lobe), and the predominantly α-helical C-terminal lobe (C-lobe) [11]. Autophosphorylation of Thr288 in the disordered T-loop (also known as the activation loop) stimulates AurA activity by stabilizing the ordered conformation of this flexible loop. This promotes the formation of the regulatory (R)-spine that connects the two lobes of the kinase domain and is characteristic of an active kinase. Binding partners, such as TPX2, efficiently stabilize the active conformation upon binding [12]. The T-loop is located on the C-lobe comprising residues 274–299, including the conserved Asp-Phe-Gly (DFG) motif, and forms the substrate binding site [13].

AurA is over-expressed in breast, colon, neuroblastoma and other cancers [6], making it an attractive drug target. Early ATP-competitive inhibitors generated against AurA were equally effective against AurB and C. More recently identified inhibitors demonstrated preferential selectivity for AurA. Alisertib (MLN8237) and LY3295668 both have marked AurA preference

(>200-fold and >1000-fold more selective, respectively, compared to AurB) and are currently being tested in Phase II and III clinical trials [14-16]. Alisertib predominantly binds at the ATP-binding pocket in a manner similar to type I inhibitors but also stabilises an inactive DFG-inter conformation. More broadly, most kinase inhibitors in clinical use, and many in pre-clinical development, target the ATP-binding site [3]. However, because this orthosteric pocket is highly conserved across kinases and kinase domains are widely utilised in signalling, ATP-competitive inhibitors frequently display poor selectivity [17]. Despite the widespread biological relevance of kinase domains, pharmacological targeting of kinases is a recurrent challenge, with many inhibitors failing clinical trials due to off-target toxicity [18].

In contrast, allosteric pockets are often more selective and are sometimes cryptic, in which a pocket only forms in a ligand-bound state through conformational change, and is not apparent in the unbound state [19, 20]. It remains challenging to identify reagents that target allosteric or cryptic sites by conventional drug discovery pathways. However, modulation at these sites offers significant advantages, particularly via their ability to accommodate selective recognition mechanisms. Allosteric inhibition has the potential to modulate activity by stabilising a subset of conformational states, as opposed to acting as a binary "on/off switch" at an orthosteric site. This fine-tuning allows more nuanced regulation of the target protein's function, enabling context-dependent modulation rather than full inhibition [23]. Synthetic binding proteins are proposed to be a class of reagent capable of overcoming this obstacle [24-27].

Synthetic binding proteins are, typically, smaller than 150 amino acid residues, consisting of a fixed scaffold that confers stability and constrains one or more variable regions. These variable regions differ in size between reagents but generate libraries capable of differentiating between small epitopes, making them ideal for allosteric site discovery [21]. Binders can be isolated from libraries using 'phage or ribosomal display methodologies or, more recently, designed *de novo* [22, 23]. Recent de novo diffusion-based binder design protocols (e.g. RFdiffusion) require predefinition of hotspot residues and known binding sites and are not currently capable of discovering cryptic or transient pockets. Although extremely powerful

when a pocket is known, they lack the ability to sample conformationally-hidden sites without a predetermined interface specification [24]. Synthetic binding proteins have previously been used to modulate AurA with some success, notably a variable new antigen receptor (vNAR) single domain antibody that overlapped the TPX2-binding site and inhibited allosterically [25]. Monobodies have also been developed as specific AurA kinase modulators, either activating or inhibiting based on their mode of interaction across the TPX2-binding site [26].

Herein, we identify and characterize Adhirons (previously known as Affimer type II), alternative synthetic binding proteins, selected due to their small probe surface formed by one or two variable regions [22, 27, 28]. Adhirons are established reagents for identifying epitopes in protein inhibition, discovering drug-binding hotspots and selectively differentiating between structurally similar targets [21, 29-33]. We isolated Adhirons against AurA using 'phage display, identifying reagents that inhibit kinase activity through a novel mechanism. We demonstrate the ability of these reagents to selectively inhibit protein kinase activity *in vitro* and *in cellulo*. X-ray crystallography revealed the mechanism of inhibition was via a previously unidentified cryptic binding pocket on the α G-Helix of the AurA C-lobe. This site has a modulatory effect on the canonical T-loop that regulates protein kinase activity, herein referred to as the 'T-pocket'. We demonstrate that Adhiron reagents provide selective inhibition of AurA in cells, while maintaining localization to the mitotic spindle in complex with TPX2.

Our work demonstrates the potential of Adhiron reagents as high affinity, selective binders capable of modulating AurA *in vitro* and *in cellulo*, offering potential as pharmacophore templates, drug discovery aids and versatile research tools.

Results:

Biochemical characterisation identifies Adhirons that bind, inhibit and stabilize AurA

Sixty unique single-looped Adhiron reagents were isolated by 'phage display against three AurA variants: full-length wild-type (residues 1-403), mutant D274N (residues 1-403) as well as the kinase domain wild-type (residues 122-403). Target-specific binding was confirmed by 'phage ELISA against immobilised AurA wild-type kinase domain (residues 122-403) (Fig. 1a). This truncation lacks the disordered N-terminus of AurA and is therefore more stable [22]. Each unique Adhiron shared a common amino acid motif, consisting of FXWX (X indicates any amino acid), suggesting that the Adhirons were interacting with a single binding epitope. Following initial pulldowns, 18 unique candidate Adhirons were assessed to analyse their effect on the thermostability of the AurA kinase domain (residues 122-403) by differential scanning fluorimetry (DSF). DSF is a valuable method in ligand and protein drug-discovery, with thermostabilising effects correlating with binding affinity or conformational change [34] [35]. Adh1, 2, 7, 19, 36 and 37 had a significant thermostabilising effect on AurA (p < 0.0001) (Fig. 1b) when compared with Adhiron scaffold control, in which the two variable regions are AAAA and AAE, respectively [34, 35]. To identify whether isolated reagents inhibited AurA kinase activity, the 18 candidate Adhirons were screened at excess 100:1 molar ratios in ADP-Glo kinase activity assays (Fig 1c) [36]. All 18 Adhirons significantly inhibited AurA kinase activity (p < 0.0001) when compared to AurA only, or to the AurA with scaffold negative control which did not itself significantly alter kinase activity. To provide a comparison with an exemplar small molecule AurA inhibitor, Alisertib (MLN8237) was used as a positive control at the same molar excess. A panel of the six most inhibitory Adhirons also significantly inhibited AurA kinase activity at 8:1 molar ratios (Fig 1d), particularly Adhirons 1 and 7 which also provided the greatest thermostabilising effect.

Adhirons 1 and 7 are potent, high-affinity inhibitors of AurA.

An ADP-Glo kinase assay was used to assess the inhibitory potency of Adhirons 1 and 7 (**Fig. 2a-b**), over AurA concentrations decreasing from 2.5 μ M to 9.31 fM. IC₅₀ values of 0.73 nM \pm 0.82 nM and 0.28 nM \pm 0.27 nM, were obtained for Adhiron 1 and 7, respectively. Subsequently, surface plasmon resonance (SPR) was performed to determine the binding kinetics of the interactions between AurA and Adhirons 1 or 7 (**Fig. 2c-d**). Adhirons were assayed at concentrations from 6.25 μ M down to 97.6 fM, demonstrating high affinities with K_D values for Adhiron 1 and 7 of 2.32 \pm 0.025 and 1.78 \pm 0.017 nM, respectively. Both reagents associated at a steady rate, K_a = 2.84 x10⁶ \pm 0.48 x10⁶ M⁻¹ min⁻¹ and 2.25 x10⁶ \pm 0.14 x10⁶ M⁻¹ min⁻¹, whereas the dissociation rates were especially slow with K_d values of 6.593 × 10⁻³ \pm 1.182 × 10⁻³ min⁻¹ and 4.01 × 10⁻³ \pm 2.066 × 10⁻⁴ min⁻¹. The Adhiron scaffold control had no detectable binding to AurA (**Supp Fig. 1**).

Crystallography elucidates the mechanism of inhibition via a novel pocket located proximally to the kinase T-loop.

Crystal structures of Adhiron 7 (**Fig. 3a**) and Adhiron 1 (**Supp Fig. 2a**) were obtained in complex with AurA (residues 122-403, containing the stabilising mutations C290A and C393A [37]) to limiting resolutions of 2.1 Å for Adhiron 7 (PDB: 9GUC) and 2.4 Å for Adhiron 1 (PDB: 9GVZ; data collection and refinement statistics summarised in **Supp Table. 1**). In these structures, AurA adopted a canonical kinase fold, with the ATP-binding pocket between the N and C-lobe occupied by an ADP molecule. As expected, due to motif similarity in the variable region, both Adhirons interacted at the same site on the α G-helix underneath the T-loop. Both Adhirons interacted primarily with residues Y334 and Y338 on AurA using F40 and W42 aromatic residues in the common Adhiron motif, as well as the Adhiron scaffold residue W70, through π – π stacking. In addition to this main site, the Adhiron:AurA binding footprint spans the α G and α EF-helices of the C-lobe (**Fig. 3a**), packing against the activation or T-loop and residue L289 in the P+1 pocket, a hydrophobic groove adjacent to the catalytic site that

anchors the P+1 residue of substrate peptides ensuring efficient orientation for phosphate transfer [11]. A notable non-substrate peptide interaction at this site is the insertion of the W77 side chain of N-Myc [38]. AurA containing the C290A and C393A stabilising mutations was used in the crystallography, but not Adhiron screening or subsequent characterisation, therefore the contact between AurA-A290 and the Adhiron scaffold in the X-ray structure provides minimal contribution to this interaction.

In complex with either Adhiron, the AurA-E181 side chain could not be modelled due to a lack of density in that region, indicating disruption of the E181–K162 salt bridge (Fig. 3b), which is a hallmark of the inactive state [39]. In addition, the side chain of Q185, part of the R-spine, does not form a hydrogen bond with the main chain of L194, the gatekeeper residue. The distance between the Q185 side chain amide and the L194 backbone carbonyl is over 4.5 Å, which is too far for H-bonding. In the active TPX2-bound structure (PDB: 10L5) [10], this distance is 3.2 Å, and the interaction is present. The absence of this hydrogen bonding in Adhiron-bound AurA indicates that the R-spine has not been assembled and the kinase is inactive. Inactive states of AurA typically have a 'DFG-Inter' conformation, in which the Phe disrupts the E181-K162 salt bridge. Although the salt bridge is also disrupted in the Adhiron-AurA crystal structures, the kinase exhibits an active 'DFG-In' conformation as seen in active kinase structures, where the Asp coordinates a magnesium ion that interacts with the βphosphate of ATP. 'DFG-In' is commonly seen with type I kinase inhibitors that bind the ATP pocket [40]. However, the Adhirons bind at a distinct allosteric site, suggesting that they are type IV inhibitors. These are typically more selective, as they bind outside conserved catalytic regions and inhibit through conformational change rather than direct competition with ATP [41]. Whilst several variable loop residues are peripheral to the interface, L47 (Adh1) / I47 (Adh7) pack into a hydrophobic groove on Aurora A at the rim of the P+1-adjacent pocket, increasing nonpolar burial at the interface. In this context, F40 from the variable loop inserts directly into the hydrophobic pocket, occupying a position equivalent to W77 of N-Myc in the AurA:N-Myc crystal structure (PDB: 5G1X) [42].

A large portion of the T-loop, G276 – T287 (Adhiron 7) and W277 – T287 (Adhiron 1), is not modelled due to lack of density, suggesting that the T-loop is flexible and not in a stabilised orientation. Our data demonstrates that the binding of Adhiron to AurA disrupts the formation of an ordered T-loop, resulting in allosteric kinase inhibition. Whether the T-loop is completely destabilised or forms an atypical Alisertib bound-like conformation, cannot be ascertained from our structural studies [43].

The hydrophobic P+1 pocket, which is adjacent to the Adhiron-binding site, contacts residues in the substrate peptide and forms part of the AurA interaction with the transcription factor and oncoprotein N-Myc [42]. N-Myc binding at the P+1 pocket occurs in neuroblastoma cells, protecting N-Myc from ubiquitination and promoting excess N-Myc accumulation [8]. However, our structural data indicates a conformational shift in core interacting residues compared to known AurA:N-Myc structures. Notably, Y334 is not in a 'flipped-out' orientation in Adhiron bound structures, demonstrating the formation of the Adhiron interaction pocket (**Fig. 3c**). Y338 also appears to shift downward in comparison to the N-Myc structure, with the binding of the Adhiron inducing a sizable conformational change at this site, 'flipping-in' Y334, and revealing a novel pocket.

There are several known binding pockets of AurA alongside the ATP-binding pocket. Several of these mediate the AurA:TPX2 interaction, including the Y, W and F pockets (**Fig. 3d**; coloured yellow, magenta and orange, respectively) [10] [44]. This allosteric binding site, is termed the T-pocket due to proximity and modulation of the canonical activation or T-loop, is adjacent but separate to the P+1 pocket.

Expression of inhibitory Adhirons caused abnormal mitosis and cell death

Inhibition of AurA causes mitotic delays. We therefore assessed mitotic progression after transient expression of TurboGFP-tagged Adhiron 1 and 7 in HeLa cells to determine if Adhirons maintain their inhibitory capabilities *in cellulo*. To assess mitotic progression, nuclear

envelope breakdown (NEB) (**Fig. 4a**) was defined as the first time point (0' min) at which chromatin condensation was visible. Metaphase plate formation was recorded for each dataset as the time-point where chromosomes aligned at the cell's equatorial plane. Anaphase onset was recorded as the first time-point showing clear separation of sister chromatids moving towards opposite poles (**Fig. 4a**). Expression of inhibitory Adhirons led to a significant increase in mitotic duration when compared to scaffold-expressing negative control cells (\bar{x} values (min): Scaffold = 40.13; Adhiron 1 = 312.10 and Adhiron 7 = 286.60; **Fig. 4a-d**). While normal bipolar mitosis was the most common recorded outcome in our live imaging experiments, there was an upward trend in incidence of tripolar mitosis (Scaffold = 0.83%; Adhiron 1 = 32.50% and Adhiron 7 = 20.83%) and incomplete mitosis (Scaffold = 0.00%; Adhiron 1 = 10.83% and Adhiron 7 = 15.83%) with both inhibitory Adhirons (**Fig. 4e**).

To explore whether the mitotic defects elicited by Adhiron 1 and 7 resulted in cell death, as previously observed following AurA inhibition, we used flow cytometry to quantitate apoptosis. We assessed staining for annexin V/propidium iodide, markers of early apoptosis and dead cells, in HeLa cells following transfection of Adhiron 1 (**Fig. 4f**; powder pink datapoints) and Adhiron 7 (**Fig. 4g**; hot pink datapoints). Both populations underwent a significant shift from live cells (quadrant; Q4) to cells either in early apoptosis (binding annexin V; Q3) or dead cells (propidium iodide staining), when compared to the Adhiron scaffold control (blue). After 72hr of transfection (**Fig. 4h**), there was a significant decrease in the number of living cells following expression of either Adhiron 1 (p=0.0003) or 7 (p=0.0003) when compared with scaffold control. This is consistent with the increased percentage of annexin V positive cells (**Fig. 4i**; Adhiron 1 p=0.0009, Adhiron 7 p=0.0006), confirming that expression of AurA-inhibitory Adhirons in HeLa cells induced apoptosis and cell death.

Adhirons 1 and 7 selectively inhibit AurA over AurB, both in vitro and in cell.

Generating inhibitors with selectivity for AurA over AurB is challenging, and almost all known small molecule AurA inhibitors inhibit both kinases [45]. To determine the selectivity of our AurA-inhibitory Adhirons, we focused on the two residues essential for the Adhiron interaction at the T-pocket in our structural characterisation, Y334 and Y338 (**Fig. 3a**). We conducted a structure-based sequence alignment (using the KinCoRe platform) which revealed that residue Y334 is not conserved, being replaced by a His in both AurB and AurC, whereas Y338 is fully conserved [46](**Fig. 5a**). Structural alignment of AurB (PDB: 4AF3) against the AurA:Adhiron 7 complex (9GUC) indicated the orientation of the histidine (H226) residue to mimic the position of Y334. We therefore assessed if Adhiron 1 and Adhiron 7 could inhibit AurB kinase activity using the ADP-Glo assay at 100x molar excess for all reagents. This indicated that Adhiron 7 had no significant effect (p= 0.5788) on AurB kinase activity, whereas Adhiron 1 reduced kinase activity by 23.1% (p= 0.0010), compared to the ~80% inhibition caused by Alisertib (p= <0.0001), a known selective AurA inhibitor, and AMG900 (p= <0.0001), a pan-Aurora kinase inhibitor (IC50 values AurA = 5 nM, AurB = 4 nM and AurC = 1 nM)[47].

In vitro selectivity against recombinant targets does not always recapitulate specificity in cells. We therefore used STED microscopy to assess colocalisation of recombinantly-produced TurboGFP-tagged Adhirons as labelling reagents for either endogenous AurA or AurB in fixed HeLa cells (**Fig. 5b**). The Adhiron scaffold showed no binding, whereas both Adhiron 1 and Adhiron 7 localised to the spindle poles, colocalising with antibody staining for endogenous AurA (indicated by white puncta, **Fig. 5b**). Colocalisation was not observed between Adhirons 1 or 7 and endogenous AurB, which localised to the kinetochores (**Fig. 5b**). These results indicate specificity of Adhiron 1 and 7 as AurA labelling reagents.

To further assess if Adhirons 1 and 7 bind AurB in cells, TurboGFP immunoprecipitations (IPs) were performed from mitotically-arrested HEK293T cells 48 hr after transient transfection with TurboGFP-Adhiron constructs (**Fig. 5c-d**). Levels of protein regulator of cytokinesis 1 (PRC1)-pThr481, a marker of mitotic CDK1 activity, were comparable across all samples

demonstrating successful synchronisation. TurboGFP-tagged Adhirons 1 and 7 strongly pulled-down endogenous AurA, indicated by the relative enrichment of the IP samples (8% per lane) over input cell lysates (0.53%/16 µg) (**Fig. 5c-d**). To assess selectivity we probed for AurB, which demonstrated a low level of binding, but no enrichment over input levels. Adhirons 1 and 7 consistently showed higher specificity to AurA, matching the *in vitro* data (**Fig. 5a**). Capture of endogenous AurB protein by IP is consistent with the *in vitro* data whereby at a >100 molar excess there is a loss of specificity to AurA for Adh1. Quantification of relative enrichment from input lysates of endogenous AurA vs AurB further highlighted the specificity of reagents (**Fig. 5d**), with AurA enriched approximately two-fold compared to input levels, whereas AurB was not enriched over input levels even at high Adhiron expression levels.

Functional consequences of Adhiron-mediated AurA inhibition in cells

Immunofluorescence imaging was used to assess the effect of Adhirons on AurA and AurB activities in a biological system. HeLa cells transiently expressing TurboGFP-Adhiron constructs (comprising scaffold, Adhiron 1 or 7) were stained for levels of AurA-pT288 and the AurB substrate histone H3-pS10 (**Fig. 6a-c**). Adhiron scaffold expression showed no effect on either marker. A 30 min treatment with either AurA or AurB inhibitors, Alisertib and ZM447439, respectively, significantly decreased the phosphorylation of their respective substrate markers. In addition, Alisertib treatment elicited a significant 22% decrease in histone H3-pS10 phosphorylation, indicating off-target effects against AurB even over short treatment periods. Adhirons 1 and 7 significantly reduced AurA-pThr288 signal to a level indistinguishable from that following Alisertib treatment, demonstating similar levels of potency. However, in contrast to Alisertib, the Adhirons did not significantly affect Histone H3-pSer10. This suggests that AurA-inhibitory Adhirons selectively modulate AurA independently of AurB in this biological system, with improved selectivity over Alisertib.

We next used western blotting to validate Adhiron-mediated inhibition of AurA in cells. Alisertib is a cell permeable inhibitor and therefore affects all cells in a culture equivalently. By contrast, the presence of non-transfected cells reduces the observable dynamic range of Adhiron-mediated changes in cell-population wide analyses. This renders direct comparison between Alisertib treatment and transiently-transfected Adhirons 1 and 7 challenging. Therefore, prior to harvesting and Aurora-A inhibitor treatment, mitotically-arrested cells were FACS-sorted to isolate TurboGFP-positive cells. Western blotting analysis of this population confirmed that both Alisertib and Adhirons 1/7 cause a complete loss of AurA-pT288 in cells (**Fig. 6d-e**).

We next examined the localisation of nuclear mitotic apparatus protein (NuMA), which AurA phosphorylates to faciliate its transport away from the spindle poles to the cell cortex [48-50]. Consistently, levels of NuMA at the spindle pole significantly increased following treatment with either Alisertib or Adhirons 1 or 7, with no significant difference between these three conditions (**Fig. 6f-g**). There was normal NuMA distribution following treatment with scaffold only negative control, or scaffold with AurB inhibitor (ZM447439). These data confirm that Adhirons prevent AurA autophosphorylation in cells.

Both Alisertib treatment and CRISPR/Cas9-mediated genomic editing have previously highlighted the importance of autophosphorylation in facilitating efficient spindle recruitment of AurA [51, 52]. As expected, we found that 30 min Alisertib treatment signifiantly decreased AurA intensity at the spindle. Surprisingly, expression of neither Adhiron 1 nor 7 triggered a reduction in AurA spindle recruitment. Instead, we observed that AurA levels on the spindle were elevated with Adhiron 1 compared to the Adhiron scaffold control (**Fig. 6f, h**). These data suggest Adhirons inhibit AurA in a manner that does not impair TPX2-mediated spindle localisation, despite ablation of AurA autophosphorylation.

Therefore, to assess changes in AurA:TPX2 association following Adhiron transfection, we developed a series of proximity ligation assays (PLA). In cells expressing Adhiron scaffold control, AurA:TPX2 PLA foci were observed across the mitotic spindle, whereas treatment with Alisertib significantly reduced PLA foci intensity by ~70% (**Fig. 7a-b**). Strikingly, the intensity

of AurA:TPX2 PLA foci was strongly increased by ~70 or ~40% following transfection of Adhirons 1 or 7, respectively (**Fig. 7a-b**). Immunofluorescent signal levels for PLA are semi-quantitative due to an enzymatic amplification step but, nevertheless, our data is consistent with the elevated or unchanged levels of AurA observed on the spindle following transfection with Adhirons 1 and 7, respectively (**Fig. 6f-h**). Subsequently, we further interogated the ability of Adhirons to impair TPX2-mediated AurA autophosphorylation using *in vitro* kinase assays, by incubating dephosphorylated AurA C290A C393A protein complexed to Adhirons and/or the AurA-activating segment of TPX2 (TPX21-56). The presence of TPX21-56 triggered a ~14-fold increase in AurA-pT288 autophosphorylation when compared to incubation of AurA alone (**Supp Fig. 4**). The addition of Adhiron scaffold did not significantly alter this response. However, Adhirons 1 and 7 completely abrogated the ability of TPX21-56 to induce increased levels of AurA-pT288 autophosphorylation, confirming that Adhirons inhibit AurA autophosphorylation even in the presence of TPX2, a potent activator of AurA.

The co-localisation of Adhirons and AurA to the spindle, in combination with PLA data for AurA:TPX2 complexes (**Fig 6f and 7a-b**), suggests that a ternary complex forms between these three proteins. To evaluate this hypothesis, we performed fluorescence anisotropy assays by incubating FITC-labelled TPX2₁₋₄₃ with various concentrations of pre-formed Adhiron:AurA complex. This resulted in increased anisotropy, indicating strong binding between TPX2 and the Adhiron:AurA complexes with K_D values of 236 ± 151 nM and 333 ± 101 nM for Adhiron 1- and 7-bound AurA, respectively (**Fig 7c**). Importantly, this increase in anisotropy is observed at concentrations higher than the single digit nanomolar K_D measured for the Adhiron:AurA complex, consistent with TPX2₁₋₄₃ associating to form a ternary complex. Together, these data indicate that Adhiron-bound AurA is still recruited to the spindle in a TPX2-dependent manner.

In the absence of AurA autophosphorylation, AurA:TPX2 complexes retained some activity against substrates in cells [50]. Therefore, although Adhirons prevent TPX2-mediated autophosphorylation of AurA, the kinase may demonstrate activity against other targets. To

test this possibility we quantified changes in two known AurA susbtrates, LATS2-pS83 and TACC3. In cells expressing Adhiron scaffold control, LATS2-pS83 was strongly present at the centrosomes, as previously described [53] whereas TACC3 was markedly enriched along the spindle (Fig 7d-f). Spindle localisation of TACC3 requires AurA-dependent phosphoryation that mediates complex formation with clathrin and chTOG [54-56]. The localisations of both LATS2-pS83 and TACC3 were unaffected by treatment with AurB inhibitor. Treatment with Alisertib or transfection of Adhirons 1 or 7 both greatly reduced levels of LATS2-pS83 and near-abolished TACC3 spindle recruitment (**Fig 7d-f**). These data confirm that Adhirons inhibit both AurA autophosphorylation and kinase activity against other substrates.

Adhirons uncouple Aurora A localisation from activation and substrate phosphorylation

Our structural studies highlighted the overlap between the novel T-pocket and the N-Myc binding site at the P+1 pocket. We therefore analysed the buried surface area of the AurA:N-Myc and AurA:Adhiron interfaces using PISA (Fig 8a) [57]. As expected, given their occupancy of different pockets, both N-Myc and Adhirons present different profiles through this analysis. Critically, however, there are hotspots of buried surface area shared by both N-Myc and Adhirons, particularly Thr288, Leu289, Tyr334 and Gln335 (Fig 8a). This led us to speculate whether occupancy of the P+1 and T-pockets is mutually exclusive. To test this, FLAG-tagged N-Myc was transfected into HEK293T cells, independently or alongside TurboGFP-Adhiron constructs (comprising scaffold, Adhiron 1 or Adhiron 7), and levels of AurA:N-Myc complexes were assessed. Cells that expressed the Adhiron scaffold control were capable of forming AurA:N-Myc complexes, but the presence of Adhiron 1 or Adhiron 7 reduced AurA:N-Myc complex formation (Fig. 8b). This indicates that Adhiron-binding in the T-pocket prevents simultaneous interaction of N-Myc at the P+1 pocket. Subsequent examination of the AurA:Adhiron-containing crystal structures aligned with AurA:N-Myc structure (5G1X)

revealed that although conserved Adhiron residue F40 occupies a similar position to N-myc:W77 in the AurA:N-Myc structure, the P+1 pocket is not properly formed in the presence of Adhirons (Fig 8c). This suggests that the unique Adhiron-mediated stabilisation of the T-pocket precludes formation of the P+1 pocket whilst occupying the proximity otherwise required for N-Myc binding. This prevents stable interaction at this site and likely impairs substrate access to, and proper orientation within, the active site.

Discussion:

We have isolated AurA-binding Adhirons which inhibit kinase activity both *in vitro* and *in cellulo*. These reagents bind with single digit nanomolar affinities for AurA and inhibit with subnanomolar IC₅₀ values for kinase inhibition (**Fig 2**), preventing both AurA auto- and substrate phosphorylation (**Fig 6 and 7e-g**).

Structural analyses demonstrated that Adhirons interact with AurA at a previously unidentified pocket that we have termed the 'T-pocket', a cryptic binding pocket on the αG-helix of the C-lobe, consisting of Y334 and Y338. Based on both *in vitro* and structural analyses, Adhiron-mediated modulation at this site inhibited kinase activity. Critically, Adhirons prevented R-spine and E181-K162 salt-bridge formation, disrupted the substrate-binding P+1 pocket through rotation of Y334 and destabilised the activation loop (**Fig. 3c, 8c-d**). The propensity to identify cryptic or unique sites has been observed in other Adhiron-based studies [29, 58, 59], highlighting a pipeline to uncover cryptic pockets to enhance drug discovery. Revealing such cryptic sites using biological tools could improve the capabilities of emerging artificial intelligence software to effectively generate allosteric inhibitors [23, 24, 60].

The Adhiron reagents characterised in this study exceed the binding affinity and potency of previously designed synthetic binding proteins that have been isolated against other sites on AurA [25, 26]. Adhirons 1 and 7 improve on the selectivity of Alisertib when used at the same dose *in vitro* (**Fig. 5b**) and even *in cellulo* (**Fig. 6a-c**). In previous studies, AurA inhibitor

treatment *in cellulo* manifested off-target effects against AurB, requiring complex experimental design and drug resistant mutations to delineate the aetiology of observed cellular phenotypes [43, 61]. We note that 30 min Alisertib treatment significantly decreased Histone H3-pS10 levels, indicating rapid onset of AurB inhibition to some degree, whereas 48 hrs of Adhiron treatment had no such effect (**Fig. 6a, c**). We suggest that T-pocket modulation of AurA activity will facilitate highly selective exploration of the biological role of AurA.

Modulation at the T-pocket both inhibits kinase activity and disrupts N-Myc binding to AurA in cells (Fig. 8b). The absence of a fully formed P+1 pocket in the Adhiron-bound AurA crystal structures suggest that the former is mutually exclusive with formation and occupancy of the T-pocket. Whilst Alisertib has been shown to perturb the N-Myc:AurA interaction due to inhibitor-induced conformational changes [8, 62], there are known off-target effects on AurB [63, 64]. Dawber et al. (2024) recently published a constrained peptide capable of orthosterically inhibiting the N-Myc:AurA interaction [65]. Whilst this approach offers a foundation for the development of reagents that perturb the N-Myc:AurA interaction, peptide delivery into cells is limited by proteolytic stability and cell permeability [65, 66]. Therefore, developing T-pocket targeting drugs based on our Adhirons may provide significant therapeutic value by disrupting the oncogenic AurA:N-Myc interaction associated with neuroblastoma, with markedly improved selectivity over Alisertib. The large and cryptic nature of the Adhiron-AurA interface underscores the novelty of the T-pocket as a druggable site. While the extensive buried surface area formed by the Adhiron cannot be fully reproduced by conventional small molecules, it defines a tractable allosteric pocket that could be exploited through structure-guided small-molecule design. In parallel, larger scaffold-based approaches may also capture elements of the Adhiron interaction surface, offering complementary strategies to achieve potency and selectivity [67]. Together, these avenues highlight the potential of the T-pocket to support novel therapeutic strategies against cancers driven by AurA dysregulation.

AurA can be considered an 'incomplete kinase' requiring binding partners for localisation and to stimulate activity [37]. Recently, we demonstrated a hierarchical relationship between AurA interactors during mitosis [50]. Firstly, CEP192-dependent centrosomal recruitment of AurA triggers autophosphorylation of the kinase. Autophosphorylated AurA has a ~10-fold greater affinity for TPX2, and therefore this centrosomal pool of AurA is primed for efficient TPX2-mediated spindle recruitment, ensuring mitotic fidelity [10, 51, 68]. Alisertib treatment perturbs TPX2-mediated spindle localisation of AurA, in part by preventing autophosphorylation (**Fig. 6-7**) [50]. Surprisingly, despite loss of autophosphorylation, both Adhirons 1 and 7 co-localised to the mitotic spindle, alongside AurA, with neither disrupting the AurA:TPX2 interaction (**Fig 7a-c**). This highlights that Adhiron-binding elicits regional, not global, conformational changes, which maintain key AurA protein-protein interactions, such as with TPX2, that are advantageous for probing Aurora kinase biology.

Since both Alisertib and Adhirons prevent AurA autophosphorylation, why does only the former impair TPX2-mediated AurA spindle recruitment? The regulatory features surrounding the AurA active site are highly dynamic, with activators and inhibitors triggering population shifts between different conformational states. Binding of TPX2 to AurA induces numerous structural changes including stabilization of the DFG-in conformation, whereas Alisertib and its analogue MLN8054 favour the DFG-inter conformation [69, 70]. Our structures indicate that Adhirons stabilize the AurA DFG-in conformation, similar to TPX2-bound AurA. As such, interaction with Adhirons, and not Alisertib, likely constrain AurA within a conformational landscape that is more compatible for TPX2 binding. Together our data demonstrates the importance of "DFG-status" in facilitating the AurA:TPX2 interaction in cells[70].

AurA:TPX2 complex formation being impacted by both autophosphorylation and "DFG-status" has interesting biological implications. The phosphatase PP6 specifically dephosphorylates AurA:TPX2 complexes, which therefore exist in both phosphorylated and dephosphorylated forms on the spindle [71]. This balance is essential to restrain AurA activity and maintain genome stability, with loss of PP6 activity and concomitant hyperactivation of AurA being

observed in melanoma [72]. Importantly, dephosphorylated AurA:TPX2 complexes retain activity against some AurA substrates including TACC3, highlighting their important catalytic role [50]. As stated above, AurA autophosphorylation triggered a ~10-fold increase in affinity for TPX2, reducing the K_D from 2.46 to 0.27 μM [47]. Although observed K_D values vary across methodologies, the latter is very similar to the K_D of ~0.3 μM measured here between TPX2 and Adhiron-bound but dephosphorylated AurA (**Fig 7**). This implies that either stabilizing the DFG-in conformation or kinase autophosphorylation causes a high affinity interaction between AurA and TPX2. This possibility could be exploited by mitotic cells. Firstly, initial loading of AurA onto spindle-bound TPX2 is autophosphorylation-dependent. TPX2-binding concomitantly stabilizes the AurA DFG-in conformation, which in turn could help maintain AurA:TPX2 complexes by preventing overly rapid dissociation following PP6-mediated dephosphorylation. This would enable more nuanced control of AurA activity, promoting genome stability through facilitating the existence of both autophosphorylated "highly" and dephosphorylated "moderately" active AurA:TPX2 complexes.

Approximately 400 proteins have been shown to specifically associate with AurA, reflecting its involvement in diverse cellular processes and disease contexts, including cancer [73]. Therefore, highly specific reagents will be invaluable for deconvoluting the interactome and understanding how AurA contributes to pathological states. Overall, our work reports the isolation and characterisation of specific reagents that have identified a novel interaction pocket, the T-pocket. Interaction at the T-pocket can modulate T-loop conformation and prevents P+1 pocket formation thereby disrupting both kinase activity and substrate binding, respectively. The AurA-inhibitory Adhirons have high selectivity, potency and affinity, a unique combination of properties that may be pharmacologically valuable. We envisage that Adhirons could serve as pharmacophore templates in structure-based drug design, whilst simultaneously offering tractable research tools to probe AurA function.

Acknowledgements

This research was supported by the Biotechnology and Biological Sciences Research Council (BBSRC) (BB/V003577/1 and BB/V003577/2). We thank Iain Manfield for use of the Biacore 1K+ (MRC)(MR/X013227/1) and his support with protein-protein interaction studies. We also thank Sally Boxall and Ruth Hughes from Leeds bioimaging facility for the use of the Cytoflex flow cytometer (BBSRC) (BB/R000352/1). We thank Francis Barr for the use of their upright microscope system.

Author contribution

J.P.R. and J.R.H. contributed equally to conceptualisation, project leadership, experimental planning, writing and editorial work. J.P.R. led biochemical, biophysical and structural investigations, including crystallographic data collection and analysis, reagent screening and isolation, construct design and protein purification, and contributed to in-cell experiments and analyses. J.R.H. led cellular investigations, including experimental design, execution, microscopy and analysis, and contributed to biochemical studies, construct design and project supervision. B.S.I. performed biochemical experiments and in-cell data analyses. I.A.M. and J.A.M. contributed to construct design, protein purification and biochemical assays, with J.A.M. also overseeing crystallisation. P.A.C. carried out STED microscopy and contributed to live-cell imaging, supervision and analysis. F.B. produced large-scale protein preparations for assays and crystallography. C.T. contributed to construct design, experimental planning, reagent isolation, supervision and mentorship. T.G.G. contributed to experimental planning and supervision. R.B. and M.W.R. contributed to construct design and crystallographic analysis. R.B., F.G., C.A.J. and D.C.T. contributed to conceptualisation, funding acquisition, supervision, experimental planning, data analysis and editorial input. C.E.L.S. contributed to project supervision.

Methods:

AurA production

Human Aurora-A kinase (AurA) variants for 'phage display screening were produced in an Nor C-terminal biotin acceptor peptide (BAP) tagged with a C terminal His tag vector (pGEX) and assays were produced from an N-terminal His-tagged vector (pET30TEV) was transformed into B834(DE3) RIL competent E. coli cells. The protein was overexpressed in LB, with growth at 37 °C until the O.D. at 600 nm reached 0.6-0.8. Expression was then induced with 0.5 mM IPTG overnight at 20 °C (BAP tagged variants had media supplemented with 50 µM of D-biotin solution). The pelleted cells were resuspended in 10 ml of ice-cold lysis buffer (50 mM Tris pH 7.5, 250 mM NaCl, 20 mM imidazole, 10% glycerol, 5 mM MgCl₂ and 200µl of Halt Protease Inhibitor Cocktail, EDTA-Free (100X) (Thermo Scientific, Cat. No. 78439)) per litre of growth culture. The resuspended cells were sonicated at 60% amplitude for 10 s on, 20 s off, 5 min total. The soluble lysate was collected at $8,000 \times g$ for 20 min in a JA 17 rotor (Beckman Coulter). After filtering (0.45 µm filter) the solution was loaded onto a 5 ml HisTrap FF column (Cytiva) equilibrated in lysis buffer. Any bound protein was eluted using a gradient of lysis buffer containing 500 mM imidazole. The His-tag was then cleaved if required overnight using TEV protease in dialysis at 4 °C into 50 mM Tris pH 7.5, 150 mM NaCl, 10% glycerol, 5 mM MgCl₂, 2 mM 2-mercaptoethanol. After dialysis the cleaved protein was rebound to the HisTrap FF column equilibrated with dialysis buffer. The AurA still interacted with the HisTrap matrix after cleavage, so a gradient of 500 mM imidazole was used to elute off the tag-free protein. The tag-free AurA was concentrated down (10 kDa cut-off concentrator, Amicon) and loaded onto a HiLoad 26/600 Superdex 200 column (Cytiva) equilibrated with 25 mM TRIS pH 7.5, 200 mM NaCl, 5 mM MgCl₂, 10% (v/v) glycerol, 2 mM 2-mercaptoethanol. In the final step, AurA was concentrated down again and flash-frozen before storage at -80 °C.

'Phage display

Adhirons against AurA were isolated by 'phage display [27]. Purified target proteins: N-tagged BAP-AurA (wildtype, residues 1-403); N-tagged BAP-AurA (D274N mutant, 1-403); C-tagged AurA-BAP (wildtype, 1-403) or N-tagged BAP-AurA (wildtype, 122-403) were immobilized on blocked (2× blocking buffer, Sigma containing 5 mM MgCl₂) streptavidin wells. The Adhiron 'phage libraries (single variable region and double variable region) were applied for 2 hr and unbound 'phage removed by 27 washes with AurA storage buffer (25 mM Tris pH 7.5, 200 mM NaCl, 5 mM MgCl₂, 10% (v/v) glycerol, 2 mM 2-mercaptoethanol) supplemented with 0.01% Tween20. Bound 'phage was eluted in a two-phase step, firstly with 0.2 M glycine pH 2.2 neutralised with 15 ml of 1 M Tris HCl, pH 9.1 and then 7.18 M triethylamine, pH 11 neutralized with 1 M Tris-HCl, pH 7. Three panning rounds were undertaken and after the final panning around 96 randomly picked colonies were used in 'phage ELISA with positive clones sent for sequencing [27]. Sixty variable regions with unique sequences were cloned into pET11 using Adhiron-His primers. AurA-binding Adhirons were produced in BL21 STAR™ (DE3) *E. coli* (Life Technologies, Invitrogen) and affinity purified using Ni-NTA resin. The cross-reactivity against AurA variants was determined by ELISA [27].

Adhiron protein production

Selected Adhiron coding regions were amplified by PCR amplification. Following *Nhel/Not*I digestion, the coding regions were ligated into a pET11a-derived vector and subsequently expressed in BL21 (DE3) cells as previously described [28]. Briefly, a single colony was used to inoculate a 5 ml overnight culture in 2TY/100 µg/ml carbenicillin. Then 50 ml LB-carb media was inoculated with 1 ml of overnight culture and grown for about 2 hr at 37°C and 230 rpm in an orbital shaker (I26 Incubator, New Brunswick Scientific) to an OD600 between 0.6–0.8, before addition of IPTG to 0.1 mM and further grown for 6–8 hr or overnight at 25°C at 150 rpm in an orbital shaker. Cells were harvested and lysed in 1 ml lysis buffer. The lysate was then incubated with 300 µl of washed NiNTA slurry for 1 hr, washed (25 mM Tris pH 7.5, 250

mM NaCl, 5 mM MgCl₂, 10% (v/v) glycerol, 20mM imidazole) and eluted in 50 mM (25 mM Tris pH 7.5, 250 mM NaCl, 5 mM MgCl₂, 10% (v/v) glycerol, 300mM imidazole).

Differential scanning fluorimetry

Thermal shift assays were performed with a QuantStudio3 real-time polymerase chain reaction (PCR) machine (Life Technologies) using SYPRO Orange dye (Invitrogen) and thermal ramping (0.3°C in step intervals between 25° and 94°C). AurA was diluted to a final concentration of 10µM in buffer (25 mM Tris pH 7.5, 200 mM NaCl, 5 mM MgCl₂, 10% (v/v) glycerol, 2 mM 2-mercaptoethanol) in the presence or absence of the 20µM scaffold control Adhiron or AurA-isolated Adhiron. Samples were assayed and data analysed using Protein Thermal Shift software v1.4 (Thermo Fisher Scientific). Normalised data were processed using the Boltzmann equation sigmoidal denaturation to generate curves, and average $T_m/\Delta T_m$ values were calculated, as previously described, using GraphPad Prism 9 software [74].

Aurora-A autophosphorylation assays

AurA 122-403 C290A C393A was purified as above with the exception that it was cotransformed into B834(DE3) RIL competent *E. coli* cells alongside pCDF- λ phosphatase, this ensures that AurA is retained in a dephosphorylated state. Dephosphorylated AurA 122-403 C290A C393A was then diluted to a concentration of 2 µM in reaction buffer (160 µM ATP, 20 mM Tris-HCl pH 7.5, 25 mM NaCl, 1 mM MgCl₂, 1 mM β-mercaptoethanol, 0.01% Tween-20). TPX2₁₋₅₆ and/or Adhiron scaffold control, 1 or 7 were then added at a 10-fold excess (20 µM). Reaction buffer was used to adjust final volumes to 120 µl. The reactions were incubated at room temperature for 90 min and stopped by the addition of 4x laemmli buffer and boiling for 10 min at 90 °C. Samples were analysed by western blot as detailed below. TPX2₁₋₅₆ was produced as follows, pGEX-GST-TPX2₁₋₅₆ was transformed into BL21(DE3) E.coli cells. The protein was overexpressed in 2xYT, with growth at 37 °C until the O.D. at 600 nm reached 0.6–0.8. Expression was then induced with 0.5 mM IPTG overnight at 20 °C. The pelleted cells were resuspended in 10 ml of ice-cold lysis buffer (50 mM Tris pH 7.5, 300 mM NaCl, 1 mM DTT and 200µl of Halt Protease Inhibitor Cocktail, EDTA-Free (100X) (Thermo Scientific, Cat. No. 78439)) per litre of growth culture. The resuspended cells were sonicated at 60% amplitude for 10 s on, 20 s off, 5 min total. The soluble lysate was collected at 8,000 \times g for 20 min in a JA 17 rotor (Beckman Coulter). After filtering (0.45 μ m filter) the solution was loaded onto a 5 ml GST resin (GE healthcare) previously equilibrated in lysis buffer. The resin was incubated for an hour at 4 °C, added to a gravity flow column and washed three times in lysis buffer. The resin was resuspended in 10 ml lysis buffer, and incubated with PreScission protease and incubated at 4 °C overnight. The resin slurry was added to a gravity flow column and the flow through, containing TPX2₁₋₅₆, collected. The column was washed with three volumes of lysis buffer, again collecting the flow through. Collected fractions were

ADP-Glo kinase assays

pooled and concentrated on 5 kDa molecular weight cut-off filter.

Single dose

An ADP-Glo assay kit (Promega) was used to screen the effect of Adhiron binding on the ATPase activity of AurA kinase or AurB kinase. 1.08 µM AurA-isolated Adhirons, Adhiron scaffold control or Alisertib (Generon) were titrated into 10 nM AurA 122–403 C290A C393A phosphorylated protein in buffer (40 mM Tris pH 7.5, 150 mM NaCl, 10 mM MgCl₂, 1 mM DTT, 0.1 mg/ml BSA, 0.01% Tween 20. Reactions were initiated by the addition of 10 µM ATP and 0.2 µg of Myelin Basic Protein (Abcam) as substrate. The reactions were incubated at room temperature for 60 min before 5 µl of ADP-Glo Reagent (Promega) was added in a white 384-well low binding plate (Corning). After a further 40 min at room temperature, 10 µl of kinase detection reagent was added to each well, and the reaction was allowed to incubate for an additional 60 min. Luminescence was measured using a fluorescence spectrometer (Tecan Spark) using a 0.5 s integration time. Control data was subtracted from the luminescence and three repeats were averaged before being plotted using GraphPad Prism 9 software.

IC₅₀ calculation

To obtain IC_{50} values the method was similar to Holder et al. [51]. Briefly, 2.5 µM of scaffold control Adhiron, Adhiron 1 or 7 were titrated with 10 nM AurA 122–403 C290A C393A phosphorylated protein in buffer as above. Reactions were initiated by the addition of 10 µM ATP and 100 µM kemptide as substrate (Cambridge Bioscience Ltd). The reactions were incubated at room temperature for 60 min before 5 µl was transferred into 5 µl of ADP-Glo Reagent (Promega) in a 384-well low volume low binding plate (Greiner Bio-one). After a further 40 min at room temperature, 10 µl of kinase detection reagent was added to each well, and the reaction was allowed to incubate for an additional 30 min. Luminescence was measured on a fluorescence spectrometer (Tecan Spark) using a 0.5 s integration time as before. Triplicates were averaged before being fitted to a sigmoidal does-response curve using GraphPad Prism 9 software. IC_{50} values were calculated by combining averages from 5 biological repeats and fitting the data to a four-parameter logistic regression model ([Inhibitor] vs. response – Variable slope).

$$Y = Bottom + \frac{(Top - Bottom)}{1 + 10^{(logIC50 - log[inhibitor]) \times Hillslope}}$$

[Inhibitor] is the concentration (not log-transformed) of Adhiron, Y is the measured response, Top and Bottom represent the upper and lower asymptotes of the curve, and the Hillslope determines the steepness of the transition.

Adhiron affinity measurements

Adhiron affinities for AurA were determined by surface plasmon resonance (SPR) using a Biacore 1K+ instrument (Cytiva). Adhiron proteins with a biotinylated C-terminal BAP-tag produced as previously described were immobilised onto streptavidin-coated CM5 sensor chips (Cytiva). Biacore experiments were performed at 25 °C in (25 mM Tris pH 7.5, 200 mM NaCl, 5 mM MgCl₂, 10% (v/v) glycerol, 2 mM 2-mercaptoethanol). AurA domain (122–403, C290A C393A) was injected at 0.0976, 0.195, 0.39, 0.78125, 1.5625, 3.125 and 6.25 nM at a flow rate of 30 μ l min⁻¹, followed by 10 min stabilisation and 30 min dissociation. The on-rates and off-rates and K_D parameters were obtained from a global fit to the SPR curves using a 1:1 Langmuir model, using the BIA evaluation software. Quoted K_D values are the mean \pm SD of three replicate measurements.

Fluorescence Anisotropy

100 nM of fluorescein isothiocyanate (FITC)-labelled TPX2 1-43 was incubated with AurA 122-403 in complex with Adhiron 1 or 7, serial diluted at a factor of 0.5 from 324 (Adhiron 1) or 160 μ M (Adhiron 7) down to 0 μ M, at a total volume of 20 μ L for 1 hr at room temperature. Assay buffer contained 25 mM Hepes pH 7.5, 150 mM NaCl, 5 mM MgCl2, 2mM DTT, and 0.01 % Tween-20 and was carried out in a flat-bottomed, black 384-well plate (Greiner Black GRE384sb plate). Fluorescence polarisation was measured using HIDEX plate reader. Data points in Figure 7c represent the mean of three technical repeats performed together; error bars indicate SD. Curves were fitted using the log(agonist) vs. response – Variable slope equation in Prism10 (GraphPad) to calculate binding affinity. The K_D reported in Figure 7c is the mean \pm SD of fitted K_D values from 3 independent experiments performed separately.

Co-expression of Adhiron 1/7 and AurA for crystallisation

His-tagged Adhiron 1 or 7 was cloned into a pET11a-derived vector with carbenicillin resistance, and human AurA domain (122–403, C290A C393A), without an epitope tag was cloned into the pCDF vector with spectinomycin resistance. Both vectors were co-transformed into *E. coli* B834 RIL cells and a 6-litre growth culture was set up. Expression was induced overnight with 0.5 mM IPTG at 20 °C. Cells were pelleted and lysed in 10 ml of lysis buffer per litre of growth media. Cells were lysed and load onto a HisTrap FF (Cytiva) equilibrated in lysis buffer and purified in the same manner as AurA (above). Purified protein underwent size exclusion chromatography, was analysed on a gel, concentrated and stored (as above).

Crystallisation and data collection

The purified Adhiron-AurA complex was concentrated to 18 mg/ml in a 10 kDa cut-off concentrator (Amicon). ADP was added to a final concentration of 5 mM and left to bind for 1 hr on ice. The complex was screened against a range of commercial crystallisation matrices. Drops were laid down at 1:1, 1:1.5 and 1.5:1 ratios of complex:precipitant in MRC sitting drop plates using a Mosquito LCP crystallisation robot (STP Labtech) and incubated at 18 °C. Rhombohedral crystals were produced using Morpheus-Fusion condition E6 (90 mM LiNaK, 1.2 % cholic acid derivative 0.1 M; Buffer System 2 (0.5M Sodium HEPES; 0.5 M MOPS (acid) pH 7.5; 30 % Precipitant Mix 1 (40% v/v PEG 500 MME; 20 % w/v PEG 20000)) as the precipitant after 2 days. Crystals were flash-frozen in liquid nitrogen. Diffraction data were collected from a single crystal at Diamond Light Source (Oxford, UK) on beamline I24. Autoprocessed data from the xia2 '3-daii' pipeline were used for structure determination (Winter, 2010). Molecular replacement was performed in PHASER (McCoy et al, 2007) using AurA 122-403 bound to N-MYC structure as a model (PDB 5G1X; (Richards et al, 2016)). Clear difference density was observed for Adhirons 1 and 7, and this was modelled in using Coot (Emsley et al, 2010). Subsequent rounds of iterative refinement were performed using REFMAC (Vagin et al, 2004) and Coot (data collection and refinement statistics can be found in Appendix Table S1). MolProbity was used to determine structure quality (Williams et al,

2018). Key contributions to the interaction between AurA and Adhiron were identified by analysis of the structure using PDBePISA (Proteins, Interfaces, Structures and Assemblies, (Krissinel and Henrick, 2007)). Structures of AurA bound to either Adhiron 1 or 7 were individually submitted to the KinCoRe server (Modi and Dunbrack, 2022) to determine the conformation of the kinase (**Supp Fig. 3a**).

Cell culture

The following cell lines were used for this study: HeLa and HEK293T, all lines tested negative for mycoplasma, and STR genotyping was used to confirm the identities of HEK293T. Both were grown in Dulbecco's modified Eagle medium (DMEM) (Sigma, D6429) supplemented with 10% heat-inactivated foetal bovine serum (FBS) (ThermoScientific 10270-106), All cells were incubated at 37 °C, 5% CO2. All cells were maintained at 37 °C in 5% CO₂.

Live cell imaging

HeLa cells were seeded into 96-well Viewpoint imaging plates (Perkin Elmer) and after 24 hr were transiently transfected with pCMV6 TurboGFP-Adhiron constructs using X-tremeGENE 9 reagent (Roche) according to manufacturer's instructions. To minimise cell death caused by excessive Adhiron TurboGFP production, pCMV6 plasmid DNA was diluted 1:4 with an inert pBluscript plasmid prior to assembly of transfection complexes. Medium was changed 4 hr after transfection and after a further 20 hr was replaced with fresh medium containing 2.5 mM thymidine. 18hr after thymidine addition, cells were washed twice with DPBS, twice with culture medium and then cultured for a further 6hr in standard medium. The medium was then replaced with CO₂-independent medium (ThermoFisher) containing 2mM glutamine, 10% FCS and SpyDNA-650 (Spirochrome, used at 1x according to the manufacturer's instructions) and cells were transferred to the plate holder of an ImageXpress Pico device (Molecular Devices) preheated to 37 °C. Image acquisition was initiated 9 hr after thymidine removal. Brightfield, GFP and CY5 epifluorescence images were captured every 5 min for a total of 12 hr with a

20x/0.4NA air objective. Three wells were imaged for each Adhiron (Adhiron 1, Adhiron 7 and Adhiron scaffold control) and the complete experiment was repeated a total of three times.

Annexin V-FITC/PI staining

Annexin V-fluorescein isothiocyanate (FITC)/propidium iodide (PI) kit (Abcam, UK - ab14085) was used to investigate Adhiron-induced apoptosis. HeLa cells were transfected with 1 µg of TurboGFP-Adhiron DNA construct in a 3:1 ratio with X-tremeGENE™ 9 DNA Transfection Reagent (Roche). Transfection complexes were left to form for 15 min at room temperature (25 °C) before being added to 6-well plates with 150,000 cells (seeded 24 hr previously) and being left to incubate at 37 °C, 5% CO₂. After 4 hr, cells were washed twice with DPBS, given fresh medium and left to incubate a further 68 hr (72 hr in total). After incubation, the cells were trypsinised, washed twice with medium and twice with DPBS, and resuspended in 500 µl of 1× binding buffer II (Abcam, UK). Then, 5 µl annexin V-FITC conjugate and 5 µl Pl were added, and the cells were incubated in the dark at room temperature for 15 min. The samples were then analysed using a CytoFLEX S Flow Cytometer (Beckman Coulter Life Sciences) which was gated for GFP-expressing cells only. Experiments consisted of three technical triplicates and three independent biological repeats.

Cell lysis and western blotting

Cells were lysed on ice for 30 min in lysis buffer (50 mM Tris pH 8.0, 300 mM NaCl, 0.2%(v/v) NP-40, 10%(v/v) glycerol, protease inhibitor cocktail C, phosphatase inhibitor cocktail 3 (Sigma, 1:200 dilution), 100 nM okadaic acid (Enzo, ALX-350-003-C100)). Lysates were then centrifuged at 14,000 × g, 15 min, 4 °C, the supernatants were transferred to a fresh tube, and the pellet was discarded. Protein concentrations were measured by Bradford assay using Protein Assay Dye Reagent Concentrate (Bio-Rad Laboratories, 5000006). NuPAGE LDS sample buffer, supplemented with NuPAGE sample reducing agent (Invitrogen) were added prior to boiling for 10 min at 90 °C. Equal amounts of protein were loaded into pre-cast 4–12% Bis-Tris gels (Invitrogen, NP0322BOX) and proteins separated in 1x MOPS buffer (Invitrogen) and transferred to nitrocellulose membranes

were then blocked in 5% [w/v] non-fat skimmed milk powder in TBS, 0.1% Tween (v/v) (TBST) for 1 h. Primary and secondary antibodies were diluted in 5% milk, TBST and incubated overnight at 4 °C or for 1 hr at room temperature, respectively. Species-specific secondary antibodies conjugated to horseradish peroxidase (HRP) were used (anti-mouse IgG, Cytiva NA931V; anti-rabbit IgG, Cytiva NA934; anti-sheep IgG, Jackson 713-035-003). Membranes were washed for 1 hr in TBST, changing the buffer five times, after each antibody incubation. All western blots were visualised using ECL (Pierce, 32106) on autorad films or, where required for weaker signals, Westar Supernova (Cyanagen, XLS3-0100).

TurboGFP-Adhiron pull-down assays

2 x 10⁶ HEK293T cells were seeded in a 15 cm dish and incubated at 37 °C, 5% CO₂ for 48 hr. Cells were then transfected as follows (per dish): 1 µg pCMV6-Adhiron-turboGFP construct + 7 μg pBluescript empty vector construct + 25 μl FuGene (Promega) + 1 ml Opti-MEM, according to manufacturer's instructions. The control transfection was carried out in the absence of any pCMV6-Adhiron-turboGFP plasmid and therefore 8 µg pBluescript construct was used. Transfected cells were incubated for 48 hr, with 100 ng/ml nocodazole (CalBiochem, 487928) added for the final 20 hr. Cells were collected by mitotic shake-off and washed twice with PBS, once with Opti-MEM and then incubated in fresh Opti-MEM for 30 minutes to rebuild mitotic spindles. Cells were then pelleted and lysed as described above. For prior washing steps all spins were at room temperature, 5 min, 400 x q and all buffers were pre-equilibrated to 37°C, 5% CO₂. For each sample, 2.8 mg of clarified lysate was taken and the volume adjusted to 300 µl before a 10 µl input sample was taken. ChromoTek TurboGFP-Trap Magnetic Agarose beads (ProteinTech - AB 2827597, 15 µl bead slurry/sample) were washed three times in lysis buffer and resuspended in 200 µl of lysis buffer per sample. Beads were added to the normalised lysates giving a final volume of 500 µl and incubated, while rotating, for 2 hr at 4°C. The beads were washed three times with lysis buffer before boiling in 20 µl 4 xNuPage LDS sample buffer, supplemented with NuPAGE sample reducing agent (Invitrogen), for 10 min at 90 °C. 30 µl of water was then added for a final

volume of 50 µl and the samples re-boiled for a further 5 min. Western blotting was carried out on lysates as described above. All beads washes were done using a magnetic rack on ice.

For immunoprecipitation assessing competition between Adhirons and N-MYC the above protocol was modified as follows. For transfection each dish received the following DNA (the remaining conditions remained the same): 1 µg pCMV6- TurboGFP-Adhiron- + 2 µg pcDNA5-Flag(CT)-NMYC + 5 µg pBluescript. The control Flag-NMYC only transfection was adjusted to contain 2 µg of pcDNA5-Flag(CT)-NMYC and 6 µg of pBluescript construct, respectively. For Flag IPs, DYKDDDDK Fab-Trap agarose (Proteintech, ffa, 15 µl/per sample) was used. Agarose washing steps required centrifugation 2500g, 5 min, 4°C. Samples were otherwise treated as above. Both Flag and TurboGFP IPs were performed from aliquots of the same input lysates.

Isolating Turbo-GFP positive populations of Adhiron transfected cells for western blot

HeLa cells were transfected with Turbo-GFP-tagged Adhiron scaffold control or Adhiron 1/7 and arrested in mitosis using nocodazole, both as described above. Cells were seeded in 6 well plates and transfection volumes and amounts were scaled down accordingly by a factor of 10. Cells were collected by mitotic shake-off and washed twice in pre-warmed PBS containing 100 ng/ml nocodazole, to maintain mitotic arrest. Cells were then FACS-sorted using BD FACSAria IIU (BD Biosciences) to collect Turbo-GFP positive cells. A non-transfected, nocodazole-arrested population of cells was used as a negative control for establishing signal gating signal thresholds. 100,000 Turbo-GFP-positive cells were collected for Adhiron scaffold control and 50,000 collected for Adhiron 1 and 7 transfections. Following sorting, cells were washed three times in Opti-MEM, pre-equilibrated to 37 °C, 5% CO₂, and incubated for 25 minutes to allow cells to rebuild mitotic spindles. When starting this incubation, the Adhiron-scaffold control cells were split in half and either DMSO control or Aurora-A inhibitor (MLN8237, 500 nM) was added, with DMSO control being added to Adhiron 1 or 7 samples. After 25 min, cells were pelleted (5 min, 400 x g) and lysed as above.

Immunofluorescence microscopy

75,000 HeLa cells were seeded in 6 well plates and simultaneously transfected as follows: 200 ng pCMV6-Adhiron-turboGFP construct + 600 ng pBluescript empty vector construct + 3 μl FuGene (Promega) + 200 μl Opti-MEM. Transfected cells were incubated for 48 hr prior to fixation in 4% paraformaldehyde for 12 min at room temperature. Coverslips for AurA and NuMA, TACC3 and LATS2-pS83 co-stainings or for Aurora-A:TPX2 proximity ligation assays were then washed once in PBS and further incubated in pre-cooled Methanol for 5 min at -20°C. For Aurora-A-pT288 and Histone H3-pS10 co-staining coverslips were quenched in 50 mM NH₄Cl for 10 min. Prior to staining all coverslips were permeabilised in 0.2 % (v/v) Triton-X100 in PBS for 5 min and then blocked in 2% BSA, 0.1% (v/v) Tween in PBS. Blocking and all antibody incubation steps were carried out for 1 hr unless otherwise stated. Primary and

secondary antibodies (Life technologies) were diluted 0.1% Tween, PBS, with secondary staining being conducted in the dark. Coverslips were gently washed three times in 0.2% Tween, PBS between antibody incubation steps. 500 ng/ml DAPI (Sigma, D9542) was included during the secondary antibody incubation to stain DNA. Coverslips were mounted on glass slides (SuperFrost Ultra Plus, Thermo Scientific) with Prolong Diamond antifade mountant (Invitrogen), allowed to cure overnight at room temperature and stored at 4°C.

A standard upright microscope system (BX61, Olympus) was used to image coverslips using GFP/Alexa Fluor 488, Cy3/Alexa Fluor 555, Cy5/Alexa Fluor 647 and DAPI filter sets (Chroma Technology Corp.). Images were taken and Z-projected using MetaMorph 7.5 imaging software (Molecular Devices) and a 2048×2048 -pixel complementary metal oxide semiconductor camera (Prim Σ , Photometrics). Illumination was provided by an LED light source (pE300, CoolLED Illumination Systems). Z-stacks were obtained at a spacing of 0.4 μ M throughout the volume of the cell.

Proximity ligation assays

Cells were seeded and fixed as above, and proximity ligation assays (PLA) carried out according to the manufacturer's instructions with the supplied buffers (Navinci, NaveniFlex Cell MR Red, NC.MR.100 Red). Samples incubations are for 1 h at 37 °C, unless otherwise stated. Coverslips were each blocked in 40 μ l blocking buffer before incubation with primary antibodies diluted in 80 μ l of primary antibody diluent. Slides were washed 3 × 5 min in TBST (TBS, 0.05% Tween) with gentle agitation. Navenibodies Mouse 1 and Rabbit 2 were diluted 1:40 in navenibody diluent (40 μ l per coverslip) and incubated with coverslips, prior to washing as above. Buffer 1 (1:5) and enzyme 1 (1:40) were diluted in water (40 μ l per coverslip) and incubated with coverslips for 30 min, prior to washing 2 × 5 min TBST. Buffer 2 red and enzyme 2 were diluted as above and incubated with coverslips for 90 min, followed by 1 × 2 min wash in TBS. Coverslips were then incubated in 1 μ g/ml DAPI in PBS for 5 min at room temperature then washed 2 × 10 min in TBS and 1 × 15 min 0.1xTBS. Slides were mounted and imaged as

described for immunofluorescence. Antibody pairs were used as follows: Aurora-A (Sigma, A1231, mouse, 1:1500) with TPX2 (Novus Biologicals, NB500-179, rabbit, 1:1500).

STED microscopy

HeLa cells were grown on No. 1.5 glass coverslips. For fixation, coverslips were washed once with warmed DPBS and then treated with warmed 3% paraformaldehyde solution in DPBS (pH 7.4) for 20 min. Cold methanol was also tested, but AurA Adhirons showed no binding using this fixation method (results not shown). After fixation, coverslips were washed three times with DPBS (10 min per wash) and then permeabilized with 0.2% TritonX-100 in DPBS at room temperature for 4 min, followed by three further DPBS washes. Cells were blocked at room temperature for 1hr using BlockAid reagent (Thermo Fisher) and then stained for 2hr with GFP-Adhiron fusions (20 µg/ml) and either rabbit monoclonal anti-AurA antibody (Cell Signalling, 1:200) or AurB mouse monoclonal antibody (BD Biosciences, 1:500) diluted in BlockAid. After two DPBS washes, cells were incubated for 1hr with secondary staining reagents diluted in BlockAid (Atto647N anti-GFP nanobodies, 1:50, Proteintech and AlexaFluor 594-labelled goat anti-mouse IgG or goat anti-rabbit IgG antibodies, 1:1000, Thermofisher). After four washes with DPBS, coverslips were mounted using Prolong Diamond Antifade mountant (Thermo Fisher). Cells were imaged on a Zeiss Axio-Observer Z1 microscope fitted with a STEDYCON system for STED imaging (University of Leeds Bioimaging Facility) using a 100x 1.4NA objective. STED resolution was set to 60nm with Nyquist sampling, and images were acquired at a single focal plane per cell (selected for maximum signal in the Adhiron channel) with the same resolution and laser power settings used for each image. Raw images were deconvolved in Huygens Professional software, optimised for processing of STEDYCON images.

Image analysis

All images were analysed in FIJI/ImageJ as described below with all figures being produced in Adobe Photoshop and Illustrator (Adobe CC).

For LATS2-pS83 intensity, a 20-pixel diameter circle was centred over each centrosome and the intensity measured. A 50-pixel diameter circle was used for NuMA and a 60-pixel diameter circle for TACC3 and Aurora-A, with a measurement from each spindle pole. For these three measurements, the circle was aligned to the edge of observable spindle pole signal. For Histone H3-pS10, a 50-pixel circle was aligned to the edge of the DAPI signal. A background intensity measurement of the same area was then taken and subtracted. For quantifying spindle and centrosomal signals, the corrected values were averaged across both centrosomes/spindle poles to produce a single value per cell.

Aurora-A-pT288 staining was imaged as part of a four-colour experiment to allow direct comparison with changes in Histone-H3pS10 (along TurboGFP-Adhiron and DAPI). These images therefore lacked a consistent spindle marker to guide placement of ROIs in the absence of Aurora-A-pT288 signal, as observed with Aurora-A inhibitor or Adhiron 1/7 treatment. Therefore, to quantify changes in Aurora-A-pThr288 signal a 180-pixel circle was placed over the centre of the cell. This ROI was sufficiently larger enough to encompass both spindle poles in control cells. The standard-deviation within this ROI was measured and used as a proxy for signal intensity. The rationale was that in control cells there would be a greater standard deviation due to the number of bright pixels containing strong Aurora-A-pT288 signal. Conversely, in Aurora-A inhibitor treated cells, the loss of Aurora-A-pT288 would result in the majority of pixels containing very similar low level signals, resulting in a greatly reduced standard deviation.

To measure the area of PLA foci, a 200-pixel circle was placed over the cell and the PLA signal intensity measured within that ROI. A 50-pixel circle was then placed in an area within the cell not containing PLA foci to generate a background intensity reading. This background intensity reading was then scaled, based on the area of ROI measured, and subtracted from the foreground measurement.

Densitometric quantification of western blots was also performed in ImageJ. Intensity was measured in a rectangular region of interest (ROI) around each band. The same size ROI was used within experiments. An adjacent region was also measured to account for background intensity.

Statistical analysis

Data were analysed in Prism v9.1.0 (GraphPad Software). Data presented are mean \pm SEM unless otherwise stated. Details of individual statistical tests are provided in figure legends. Normal distribution of the data was processed as standard GraphPad (D'Agostino-Pearson omnibus test). The one-way analysis of variance (ANOVA) (Girden, 1992) with Dunnett's post-hoc test was performed to assess statistical significance between three or more datasets, unless otherwise stated. The Student's paired t-test (Student, 1908) with two-tailed distribution was used for comparisons of two data sets with normal distributions. p values were assigned to summarise pairwise comparisons of statistical significance. Significance thresholds: ns (not significant; p > 0.05), * ($p \le 0.05$), ** ($p \le 0.01$), **** ($p \le 0.001$), ***** ($p \le 0.0001$).

References:

- 1. Bhullar, K.S., et al., *Kinase-targeted cancer therapies: progress, challenges and future directions.* Molecular Cancer, 2018. **17**(1): p. 48.
- 2. Müller, S., et al., *The ins and outs of selective kinase inhibitor development.* Nature Chemical Biology, 2015. **11**(11): p. 818-821.
- 3. Arter, C., et al., Structural features of the protein kinase domain and targeted binding by small-molecule inhibitors. J Biol Chem, 2022. **298**(8): p. 102247.
- 4. Mingione, V.R., et al., *Allosteric regulation and inhibition of protein kinases*. Biochem Soc Trans, 2023. **51**(1): p. 373-385.
- 5. Du, R., et al., *Targeting AURKA in Cancer: molecular mechanisms and opportunities for Cancer therapy.* Molecular Cancer, 2021. **20**(1): p. 15.
- 6. Nikonova, A.S., et al., *Aurora A kinase (AURKA) in normal and pathological cell division.* Cellular and Molecular Life Sciences, 2013. **70**(4): p. 661-687.
- 7. Park, J.-G., et al., *Structural basis for CEP192-mediated regulation of centrosomal AURKA*. Science Advances, 2023. **9**(16): p. eadf8582.
- 8. Otto, T., et al., *Stabilization of N-Myc is a critical function of Aurora A in human neuroblastoma*. Cancer Cell, 2009. **15**(1): p. 67-78.
- 9. Burgess, S.G., et al., *Mitotic spindle association of TACC3 requires Aurora-A-dependent stabilization of a cryptic* α *-helix.* Embo j, 2018. **37**(8).
- 10. Bayliss, R., et al., Structural Basis of Aurora-A Activation by TPX2 at the Mitotic Spindle. Molecular Cell, 2003. **12**(4): p. 851-862.
- 11. Levinson, N.M., *The multifaceted allosteric regulation of Aurora kinase A.* Biochemical Journal, 2018. **475**(12): p. 2025-2042.
- 12. Littlepage, L.E., et al., *Identification of phosphorylated residues that affect the activity of the mitotic kinase Aurora-A.* Proceedings of the National Academy of Sciences, 2002. **99**(24): p. 15440-15445.
- 13. Nolen, B., S. Taylor, and G. Ghosh, *Regulation of Protein Kinases: Controlling Activity through Activation Segment Conformation*. Molecular Cell, 2004. **15**(5): p. 661-675.
- 14. Zhou, N., et al., *The Investigational Aurora Kinase A Inhibitor MLN8237 Induces Defects in Cell Viability and Cell-Cycle Progression in Malignant Bladder Cancer Cells In Vitro and In Vivo.* Clinical Cancer Research, 2013. **19**(7): p. 1717-1728.
- 15. Du, J., et al., Aurora A–Selective Inhibitor LY3295668 Leads to Dominant Mitotic Arrest, Apoptosis in Cancer Cells, and Shows Potent Preclinical Antitumor Efficacy. Molecular Cancer Therapeutics, 2019. **18**(12): p. 2207-2219.
- 16. Chu, Q.S.-c., et al., *Aurora kinase A inhibitor, LY3295668 erbumine: a phase 1 monotherapy safety study in patients with locally advanced or metastatic solid tumors.* Investigational New Drugs, 2021. **39**(4): p. 1001-1010.
- 17. Uitdehaag, J.C., et al., *Comparison of the cancer gene targeting and biochemical selectivities of all targeted kinase inhibitors approved for clinical use.* PLoS One, 2014. **9**(3): p. e92146.
- 18. Hantschel, O., *Unexpected Off-Targets and Paradoxical Pathway Activation by Kinase Inhibitors*. ACS Chemical Biology, 2015. **10**(1): p. 234-245.
- 19. Vajda, S., et al., *Cryptic binding sites on proteins: definition, detection, and druggability.* Curr Opin Chem Biol, 2018. **44**: p. 1-8.
- 20. Cimermancic, P., et al., *CryptoSite: Expanding the Druggable Proteome by Characterization and Prediction of Cryptic Binding Sites.* Journal of Molecular Biology, 2016. **428**(4): p. 709-719.
- 21. Martin, H.L., et al., *Non-immunoglobulin scaffold proteins: Precision tools for studying protein-protein interactions in cancer.* New Biotechnology, 2018. **45**: p. 28-35.
- Tang, A.A.-S., et al., *Isolation of isoform-specific binding proteins (Affimers) by phage display using negative selection.* Science Signaling, 2017. **10**(505): p. eaan0868.

- 23. Chevalier, A., et al., *Massively parallel de novo protein design for targeted therapeutics.* Nature, 2017. **550**(7674): p. 74-79.
- 24. Watson, J.L., et al., *De novo design of protein structure and function with RFdiffusion.* Nature, 2023. **620**(7976): p. 1089-1100.
- 25. Burgess, S.G., et al., *Allosteric inhibition of Aurora-A kinase by a synthetic vNAR domain.* Open Biol, 2016. **6**(7).
- Zorba, A., et al., *Allosteric modulation of a human protein kinase with monobodies.* Proceedings of the National Academy of Sciences, 2019. **116**(28): p. 13937-13942.
- 27. Tiede, C., et al., *Affimer proteins are versatile and renewable affinity reagents.* eLife, 2017. **6**: p. e24903.
- 28. Tiede, C., et al., Adhiron: a stable and versatile peptide display scaffold for molecular recognition applications. Protein Eng Des Sel, 2014. **27**(5): p. 145-55.
- 29. Haza, K.Z., et al., RAS-inhibiting biologics identify and probe druggable pockets including an $SII-\alpha 3$ allosteric site. Nature Communications, 2021. **12**(1): p. 4045.
- 30. Heseltine, S., et al., *High-Throughput profiling of SH2 domains using Affimer reagents:* unravelling protein interaction networks. 2024.
- Tang, A.A.S., et al., *Targeting Grb2 SH3 Domains with Affimer Proteins Provides Novel Insights into Ras Signalling Modulation*. Biomolecules, 2024. **14**(8): p. 1040.
- 32. Hughes, D.J., et al., *Generation of specific inhibitors of SUMO-1– and SUMO-2/3–mediated protein-protein interactions using Affimer (Adhiron) technology.* Science Signaling, 2017. **10**(505): p. eaaj2005.
- 33. Robinson, J.I., et al., Affimer proteins inhibit immune complex binding to FcγRIIIa with high specificity through competitive and allosteric modes of action. Proc Natl Acad Sci U S A, 2018. **115**(1): p. E72-e81.
- 34. Niesen, F.H., H. Berglund, and M. Vedadi, *The use of differential scanning fluorimetry to detect ligand interactions that promote protein stability.* Nature Protocols, 2007. **2**(9): p. 2212-2221.
- 35. Gao, K., R. Oerlemans, and M.R. Groves, *Theory and applications of differential scanning fluorimetry in early-stage drug discovery.* Biophys Rev, 2020. **12**(1): p. 85-104.
- 36. Zegzouti, H., et al., *ADP-Glo: A Bioluminescent and Homogeneous ADP Monitoring Assay for Kinases.* ASSAY and Drug Development Technologies, 2009. **7**(6): p. 560-572.
- 37. Burgess, S.G. and R. Bayliss, *The structure of C290A:C393A Aurora A provides structural insights into kinase regulation*. Acta Crystallographica Section F, 2015. **71**(3): p. 315-319.
- 38. Richards Mark, W., et al., *Structural basis of N-Myc binding by Aurora-A and its destabilization by kinase inhibitors.* Proceedings of the National Academy of Sciences, 2016. **113**(48): p. 13726-13731.
- 39. Bayliss, R., S.G. Burgess, and P.J. McIntyre, *Switching Aurora-A kinase on and off at an allosteric site.* The FEBS Journal, 2017. **284**(18): p. 2947-2954.
- 40. Roskoski, R., *Classification of small molecule protein kinase inhibitors based upon the structures of their drug-enzyme complexes.* Pharmacological Research, 2016. **103**: p. 26-48.
- 41. Gavrin, L.K. and E. Saiah, *Approaches to discover non-ATP site kinase inhibitors*. MedChemComm, 2013. **4**(1): p. 41-51.
- 42. Richards, M.W., et al., *Structural basis of N-Myc binding by Aurora-A and its destabilization by kinase inhibitors.* Proc Natl Acad Sci U S A, 2016. **113**(48): p. 13726-13731.
- 43. Gilburt, J.A.H., et al., *Dynamic Equilibrium of the Aurora A Kinase Activation Loop Revealed by Single-Molecule Spectroscopy.* Angewandte Chemie, 2017. **129**(38): p. 11567-11572.
- 44. McIntyre, P.J., et al., Characterization of Three Druggable Hot-Spots in the Aurora-A/TPX2 Interaction Using Biochemical, Biophysical, and Fragment-Based Approaches. ACS Chem Biol, 2017. **12**(11): p. 2906-2914.
- de Groot, C.O., et al., *A Cell Biologist's Field Guide to Aurora Kinase Inhibitors.* Front Oncol, 2015. **5**: p. 285.

- 46. Modi, V. and R.L. Dunbrack, Jr, *Kincore: a web resource for structural classification of protein kinases and their inhibitors.* Nucleic Acids Research, 2021. **50**(D1): p. D654-D664.
- 47. Payton, M., et al., *Preclinical evaluation of AMG 900, a novel potent and highly selective panaurora kinase inhibitor with activity in taxane-resistant tumor cell lines.* Cancer Res, 2010. **70**(23): p. 9846-54.
- 48. Kotak, S., et al., Aurora A kinase regulates proper spindle positioning in C. elegans and in human cells. J Cell Sci, 2016. **129**(15): p. 3015-25.
- 49. Gallini, S., et al., *NuMA Phosphorylation by Aurora-A Orchestrates Spindle Orientation*. Current Biology, 2016. **26**(4): p. 458-469.
- 50. Polverino, F., et al., *The Aurora-A/TPX2 Axis Directs Spindle Orientation in Adherent Human Cells by Regulating NuMA and Microtubule Stability.* Curr Biol, 2021. **31**(3): p. 658-667.e5.
- 51. Holder, J., et al., *CEP192 localises mitotic Aurora-A activity by priming its interaction with TPX2.* The EMBO Journal, 2024. **43**(22): p. 5381-5420.
- 52. Asteriti, I.A., et al., *The Aurora-A inhibitor MLN8237 affects multiple mitotic processes and induces dose-dependent mitotic abnormalities and aneuploidy.* Oncotarget, 2014. **5**(15): p. 6229-42.
- Toji, S., et al., *The centrosomal protein Lats2 is a phosphorylation target of Aurora-A kinase.* Genes to Cells, 2004. **9**(5): p. 383-397.
- 54. Cheeseman, L.P., et al., Aurora A kinase activity is required for localization of TACC3/ch-TOG/clathrin inter-microtubule bridges. Commun Integr Biol, 2011. **4**(4): p. 409-12.
- 55. Burgess, S.G., et al., *Aurora-A-Dependent Control of TACC3 Influences the Rate of Mitotic Spindle Assembly.* PLoS Genet, 2015. **11**(7): p. e1005345.
- 56. Burgess, S.G., et al., *Allosteric inhibition of Aurora-A kinase by a synthetic vNAR domain.* Open biology, 2016. **6**(7): p. 160089.
- 57. Krissinel, E. and K. Henrick, *Inference of macromolecular assemblies from crystalline state.* J Mol Biol, 2007. **372**(3): p. 774-97.
- 58. Robinson James, I., et al., Affimer proteins inhibit immune complex binding to FcγRIIIa with high specificity through competitive and allosteric modes of action. Proceedings of the National Academy of Sciences, 2018. **115**(1): p. E72-E81.
- 59. Martin, H.L., et al., Affimer-mediated locking of p21-activated kinase 5 in an intermediate activation state results in kinase inhibition. Cell Reports, 2023. **42**(10): p. 113184.
- 60. Rettie, S.A., et al., Accurate de novo design of high-affinity protein binding macrocycles using deep learning. bioRxiv, 2024.
- 61. Sloane, D.A., et al., *Drug-resistant aurora A mutants for cellular target validation of the small molecule kinase inhibitors MLN8054 and MLN8237.* ACS Chem Biol, 2010. **5**(6): p. 563-76.
- 62. Niu, H., M. Manfredi, and J. Ecsedy, *Scientific Rationale Supporting the Clinical Development Strategy for the Investigational Aurora A Kinase Inhibitor Alisertib in Cancer.* Frontiers in oncology, 2015. **5**: p. 189.
- 63. Tayyar, Y., et al., *Critical risk-benefit assessment of the novel anti-cancer aurora a kinase inhibitor alisertib (MLN8237): A comprehensive review of the clinical data.* Critical Reviews in Oncology/Hematology, 2017. **119**: p. 59-65.
- 64. Kelly, K.R., et al., *The novel Aurora A kinase inhibitor MLN8237 is active in resistant chronic myeloid leukaemia and significantly increases the efficacy of nilotinib.* J Cell Mol Med, 2011. **15**(10): p. 2057-70.
- Dawber, R.S., et al., *Inhibition of Aurora-A/N-Myc Protein—Protein Interaction Using Peptidomimetics: Understanding the Role of Peptide Cyclization*. ChemBioChem, 2024. **25**(2): p. e202300649.
- 66. Wang, H., et al., *Peptide-based inhibitors of protein-protein interactions: biophysical, structural and cellular consequences of introducing a constraint.* Chem Sci, 2021. **12**(17): p. 5977-5993.
- 67. Tibbitts, J., et al., *Key factors influencing ADME properties of therapeutic proteins: A need for ADME characterization in drug discovery and development.* MAbs, 2016. **8**(2): p. 229-45.

- 68. Eyers, P.A., et al., *A novel mechanism for activation of the protein kinase Aurora A*. Curr Biol, 2003. **13**(8): p. 691-7.
- 69. Dodson, C.A., et al., *Crystal structure of an Aurora-A mutant that mimics Aurora-B bound to MLN8054: insights into selectivity and drug design.* Biochem J, 2010. **427**(1): p. 19-28.
- 70. Lake, E.W., et al., Quantitative conformational profiling of kinase inhibitors reveals origins of selectivity for Aurora kinase activation states. Proceedings of the National Academy of Sciences, 2018. **115**(51): p. E11894-E11903.
- 71. Zeng, K., et al., *Protein phosphatase 6 regulates mitotic spindle formation by controlling the T-loop phosphorylation state of Aurora A bound to its activator TPX2*. J Cell Biol, 2010. **191**(7): p. 1315-32.
- 72. Hammond, D., et al., *Melanoma-associated mutations in protein phosphatase 6 cause chromosome instability and DNA damage owing to dysregulated Aurora-A.* J Cell Sci, 2013. **126**(Pt 15): p. 3429-40.
- 73. Prasath Damodaran, A., et al., *Proteomic study identifies Aurora-A mediated regulation of alternative splicing through multiple splicing factors.* Journal of Biological Chemistry, 2024: p. 108000.
- 74. Byrne, D.P., et al., Aurora A regulation by reversible cysteine oxidation reveals evolutionarily conserved redox control of Ser/Thr protein kinase activity. Sci Signal, 2020. **13**(639).

Synthetic protein binders reveal a cryptic regulatory pocket on Aurora A for selective allosteric inhibition

Figure 1 Biochemical characterization identifies Adhirons that bind, inhibit and stabilize AurA

a 'phage ELISAs (corrected for background) testing 60 monoclonal Adhiron reagents identified from four independent screens of full-length AurA variants. **b** Melting temperature (T_m) measured by differential scanning fluorimetry (DSF) of 10 μ M AurA incubated with 20 μ M of 18 selected candidate Adhirons, with the Adhiron scaffold (blue) as the negative control. **c** The 18 Adhirons screened for inhibition of AurA using ADP-Glo assay at an excess 100 : 1 molar ratio (1.08 μ M Adhiron : 10.8nM AurA), with Alisertib and Adhiron scaffold (blue) as controls. **d** Inhibitory Adhirons screened for inhibition of AurA using ADP-Glo assay at 8 : 1 molar ratio (86.4nM Adhiron : 10.8nM AurA). Adhiron 1 and 7 datasets are indicated by powder-pink and hot-pink bars throughout.

Statistical analysis is one-way ANOVA, Dunnett's multiple comparisons test significance thresholds: ns (P > 0.05), * (P \leq 0.05), ** (P \leq 0.01), *** (P \leq 0.001), **** (P \leq 0.0001). vs. Scaffold Control.

Figure 2 Adhirons 1 and 7 are potent, high-affinity inhibitors of AurA

a-b ADP-Glo kinase activity assays assessing Adhiron potency for: **a** Adhiron 1, and **b** Adhiron 7. 10.8nM AurA C290A, C393A (122-403) was incubated with each Adhiron at concentrations ranging from 2500 nM down to 9.31 fM, and curves were fitted to obtain IC_{50} values. **c-d** Binding parameters measured by surface plasmon resonance (SPR) for: **c** Adhiron 1, and **d** Adhiron 7. Adhirons were immobilized on streptavidin-coated CM5 sensor chips via C-terminal biotin and challenged with decreasing concentrations (6.25 μ M down to 97.6 fM) of AurA C290A, C393A (122-403). Representative curves of three replicate experiments are shown, with experimental data indicated by coloured curves and Langmuir 1:1 fitting curves in black.

Figure 3 Crystallography elucidates the mechanism of inhibition via a novel pocket located proximally to the kinase T-loop

a Crystal structure of the Aurora-AC290A/C393A 122-403 (AurA, green cartoon) in complex with Adhiron 7 residues (hot-pink), with a magnified view of the structure with key residues shown as sticks. **b** A representative region of the 2Fo-Fc electron density map (contour: 1.0 σ) of the 2.1Å crystal structure of Adhiron 7 bound to the AurA, showing disruption of the E182-K162 salt bridge. **c** Comparative surface alignment of Y334 and Y338 in the P+1 pocket conformation of the N-Myc–AurA complex (PDB: 5G1X; N-Myc, maroon; AurA, cyan) and the Adhiron 7–AurA complex (PDB: 9GUC; Adhiron, green; AurA, hot pink). The magnified view (stick representation) shows Y334 flipping out in the N-Myc complex (deep blue) versus adopting a planar orientation in the Adhiron complex (hot pink). Y338 is also shown for both structures. **d** Crystal structure of AurA (grey, surface):ATP-binding pocket is modelled with ATP (orange sticks); TPX2 pockets: Y pocket (yellow), F (orange), and the W pocket (purple); P+1 pocket (blue) is modelled, along with the novel T-pocket (hot-pink). All models were made in Pymol.

Figure 4. Live Cell imaging observations of HeLa cells transiently transfected with Turbo-GFP tagged Adhiron 1 and 7

a Composite fluorescence of TurboGFP-Adhiron (green), DNA (magenta) and brightfield images of a representative cell transiently expressing scaffold control Adhiron. Cell cycle stages are indicated above the panels (G2, nuclear envelope breakdown (NEB), metaphase and anaphase) with times from NEB (min) indicated on brightfield images (top left). b a representative cell transiently expressing Turbo-GFP-Adhiron 1 (green) demonstrating tripolar mitosis (visualised by DNA (SpyDNA); magenta). c A representative cell transiently expressing TurboGFP-Adhiron 7 (green) demonstrating incomplete mitosis. d Time taken from NEB to anaphase onset (min) for Adhiron 1 (powder-pink) and 7 (hot-pink) compared with scaffold control (blue). e Percentage of cells progressing through bipolar mitosis (black), tripolar mitosis (folly-red) or incomplete mitosis (surfie-green) over the imaging time period (725 mins). f-g, Apoptosis assay (annexin V-FITC/PI) using flow cytometry for: f Adhiron 1 (powder-pink) overlaid with scaffold control (blue), and **g** Adhiron 7 (hot-pink) overlaid with scaffold control (blue). HeLa cells were transfected with TurboGFP-Adhiron constructs and FACS analysis was done after 72 h. Representative scatter plots of PI (yaxis) vs. annexin V (x-axis) are shown. h Percentage of live cells (Q4) for the indicated treatments. i Percentage of annexinV (Q3) cells per treatment. Data are presented as the mean ± SD of triplicate experiments. One-way ANOVA, Dunnett's correction for multiple comparisons; *** P ≤ 0.001 vs. control.

Figure 5 Adhirons 1 and 7 selectively inhibit AurA over AurB, both in vitro and in cells

a Left panel: structural alignment of AurA:Adhiron 7 complex (PDB: 9GUC; AurA in green, Adhiron in hot-pink) with AurB (PDB: 4AF3, orange) showing non-conserved Y/H residues at the 334 position, conserved Y338 and key Adhiron residues (hot-pink). The structure is based on sequence alignment of AurA, AurB and AurC from KinCoRe [15]. Right panel: Adhirons 1 and 7 screened for inhibition of AurB using the ADP-Glo assay at excess 100 : 1 molar ratio (1.08mM Adhiron : 10.8nM AurB), controlled for using AurA selective inhibitor Alisertib, pan-Aurora inhibitor AMG900 and Adhiron scaffold. Statistical analysis is one-way ANOVA, with Dunnett's multiple comparisons test **b** STED images of HeLa cells co-stained with the indicated TurboGFP-Adhiron fusions and anti-Aur antibodies. **c** Levels of endogenous AurA assessed by western blot analysis of TurboGFP-Adhiron immunoprecipitations following over-expression in HEK293 cells. Input = 0.57% and IP = 8% of total, blotted for AurA, AurB, Turbo-GFP, PRC1-pT481 and α -tubulin. **d** Quantification of western blot analysis of relative enrichment of Adhiron pulldown of endogenous AurA compared to AurB.

Adh1, Adhiron 7and Scaffold are coloured Powder-Pink, Hot-Pink and Blue throughout.

Figure 6. Functional consequences of Adhiron-mediated AurA inhibition in cells.

a Immunofluorescence images of HeLa cells transiently transfected with either Adhiron scaffold control or Adhirons 1 or 7 and treated with DMSO vehicle control, AurA inhibitor (MLN8237, 500 nM) or AurB inhibitor (ZM447439, 2 µM), as indicated, for 30 minutes prior to fixation. Antibodies against Aurora-A-pT288 and Histone H3-pS10 are red and blue in merged images, respectively, with TurboGFP-Adhiron proteins in green. DNA stained with DAPI is shown in an additional panel. Box plots of **b** Aurora-A-pT288 standard deviation or **c** Histone H3-pS10 intensity, with representative images shown in a (n=3, ≥10 cells/biological replicate). Exact p-values from **b** vs Con (L-R): <0.0001, 0.7445, <0.0001, <0.0001; vs AurA-

i: <0.0001, >0.9999, >0.9999. Exact p-values from **c** vs Con (L-R): 0.0010, <0.0001, >0.9999, >0.9999; vs AurA-i: <0.0001, 0.0110, 0.0477. **d** Western blot analysis of HeLa cells transiently transfected as in a and arrested in mitosis (100 ng/ml nocodazole for 20 hr). Cells were FACS-sorted to isolate TurboGFP positive cells, washed and incubated in nocodazolefree Opti-MEM medium for 30 min, to allow mitotic spindles to be rebuilt. During this incubation, cells were treated with either DMSO vehicle control or AurA inhibitor for 30 minutes, as in a, prior to lysis. e Densitometric quantification of Aurora-A-pT288 signal from d. Black bars indicate mean ± S.D (n = 3 biological replicates). Exact p-values from e (L-R): <0.0001, <0.0001, <0.0001. f Immunofluorescence images of HeLa cells treated as in a. Antibodies against nuclear mitotic apparatus (NuMA) and Aurora-A are red and blue in merged images, respectively, with TurboGFP Adhiron proteins in green. DNA stained with DAPI is shown in an additional panel. Box plots of **g** Aurora-A spindle or **h** NuMa spindle pole intensities, with representative images shown in \mathbf{f} (n=3, \geq 10 cells/biological replicate). Exact p-values from q vs Con (L-R): <0.0001, >0.9999, <0.0001, 0.0003; vs AurA-i: <0.0001, >0.9999, 0.3892. Exact p-values from h vs Con (L-R): <0.0001, 0.6915, 0.0001, 0.7956; vs AurA-i: <0.0001, <0.0001, <0.0001.

Box plots in (**b-c** and **g-h**) indicate the median and interquartile ranges (25th–75th percentile) with black whiskers representing 5th–95th percentile ranges. p-values are denoted as follows: ****p < 0.0001, ***p < 0.001, *p < 0.05, n.s not significant (**b-c** and **g**, Kruskal-Wallis test, **e** One-way ANOVA, **h** Brown-Forsythe and Welch correction for multiple comparisons). Scale bar in **a** and **f** represents 10 μ m.

Figure 7 Adhirons uncouple Aurora A localisation from activation and substrate phosphorylation

a Proximity ligation assay (PLA) between Aurora-A and TPX2 in HeLa cells transiently transfected with either Adhiron scaffold control or Adhirons 1 or 7 and treated with DMSO vehicle control or AurA inhibitor (MLN8237, 500 nM), as indicated, for 30 minutes prior to fixation. PLA signal is red in merged images, with TurboGFP-Adhiron protein in green and DNA stained with DAPI in blue. **b** Box plots of Aurora-A:TPX2 PLA signal from mitotic cells in a, with representative images shown in a (n=3, ≥16 cells/biological replicate). Exact pvalues from **b** vs Con (L-R): <0.0001, <0.0001, 0.0004; vs AurA-i: <0.0001, <0.0001. **c** Fluorescence anisotropy binding assay between 100 nM FITC-labelled TPX2₁₋₄₃ binding to unlabelled pre-formed AurA: Adhiron 1 (light pink) or 7 (hot pink) complexes. Displayed data points represent the mean anisotropy ±SD from 3 technical repeats within a single experiment. KD values presented are the mean ±SD of KD values calculated from 3 independent experimental repeats. d Immunofluorescence images of HeLa cells, treated as in **a**, with an additional AurB inhibitor treated condition (ZM447439, 2 µM). Antibodies against TACC3 and LATS2-pS83 are red and blue in merged images, respectively, with TurboGFP-Adhirons in green. DNA stained with DAPI is shown in an additional panel. Box plots of e LATS2-pS83 spindle pole and f TACC3 spindle intensities, with representative images shown in **d** (n=3, ≥10 cells/biological replicate). Exact p-values from **e** vs Con (L-R): <0.0001, >0.9999, <0.0001, <0.0001; vs AurA-i: <0.0001, >0.9999, >0.9999. Exact p-values from **f** vs Con (L-R): <0.0001, >0.9999, <0.0001, <0.0001; vs AurA-i: <0.0001, >0.9999, >0.9999.

Box plots in **b** and **e-f** indicate the median and interquartile ranges (25th–75th percentile) with black whiskers representing 5th–95th percentile ranges. p-values are denoted as follows: ****p < 0.0001, ***p < 0.0001, n.s not significant (**b** One-way ANOVA with Brown-Forsythe and Welch correction for multiple comparisons ANOVA; **e-f**, Kruskal-Wallis test). Scale bar in **a** and **d** represents 10 μ m.

Figure 8 Adhiron binding to the T-pocket is mutually exclusive with occupancy of the P+1 pocket

a Heat-map visualisation of Buried Surface Area analysis of the interaction interface between AurA and either N-Myc, Adhiron 1 or 7. Key relating heat-map colour with buried surface area (Å²) is shown below the map. **b** Western blot analysis of TurboGFP-Adhiron and Flag IP from HEK293T cells transfected with Flag-N-Myc in the presence or absence of TurboGFP-Adhirons, as indicated. Both Flag and TurboGFP IPs were performed from aliquots of the same input lysate. c Alignment of the area surrounding the P+1 pocket for the AurA:N-Myc (PDB: 5G1X) and AurA:Adhiron 7 (PDB: 9GUC) crystal structures. d Schematic detailing the structural features which define the different activation states of AurA. The activation loop is shown as a dotted or filled line, representing disorder and order, respectively. The phenylalanine residue indicates the orientation of the DFG-motif: DFG-in but not DFG-inter being compatible with kinase activity through proper coordination of ATP molecules. The P+1 substrate-binding pocket is a dotted outline or filled black shape when absent or formed, respectively. AurA alone (i) and inhibitor-bound (MLN8054) (ii) share the key features of inactivity, including a disordered T-loop, an improperly formed P+1 pocket and DFG-inter conformation. Whilst also inactive, Adhiron-bound AurA (iii) exists in the DFG-in state, but unlike inhibitor-bound AurA remains able to bind TPX2. Finally, AurA in complex with TPX2 (iv), has all the structural hallmarks required for an active kinase, including an autophosphorylated and ordered T-loop, formed P+1 pocket and presenting a DFG-in conformation.

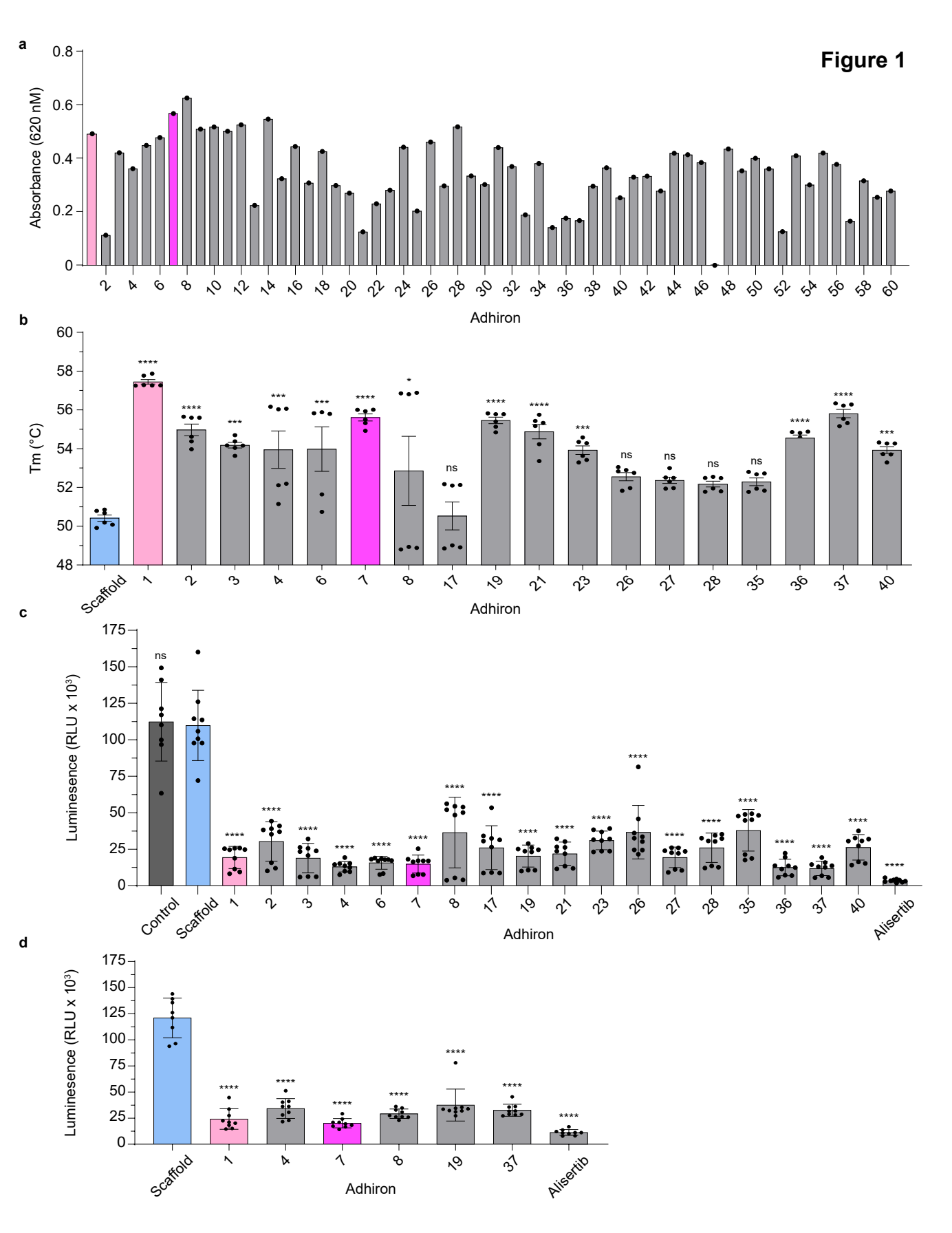
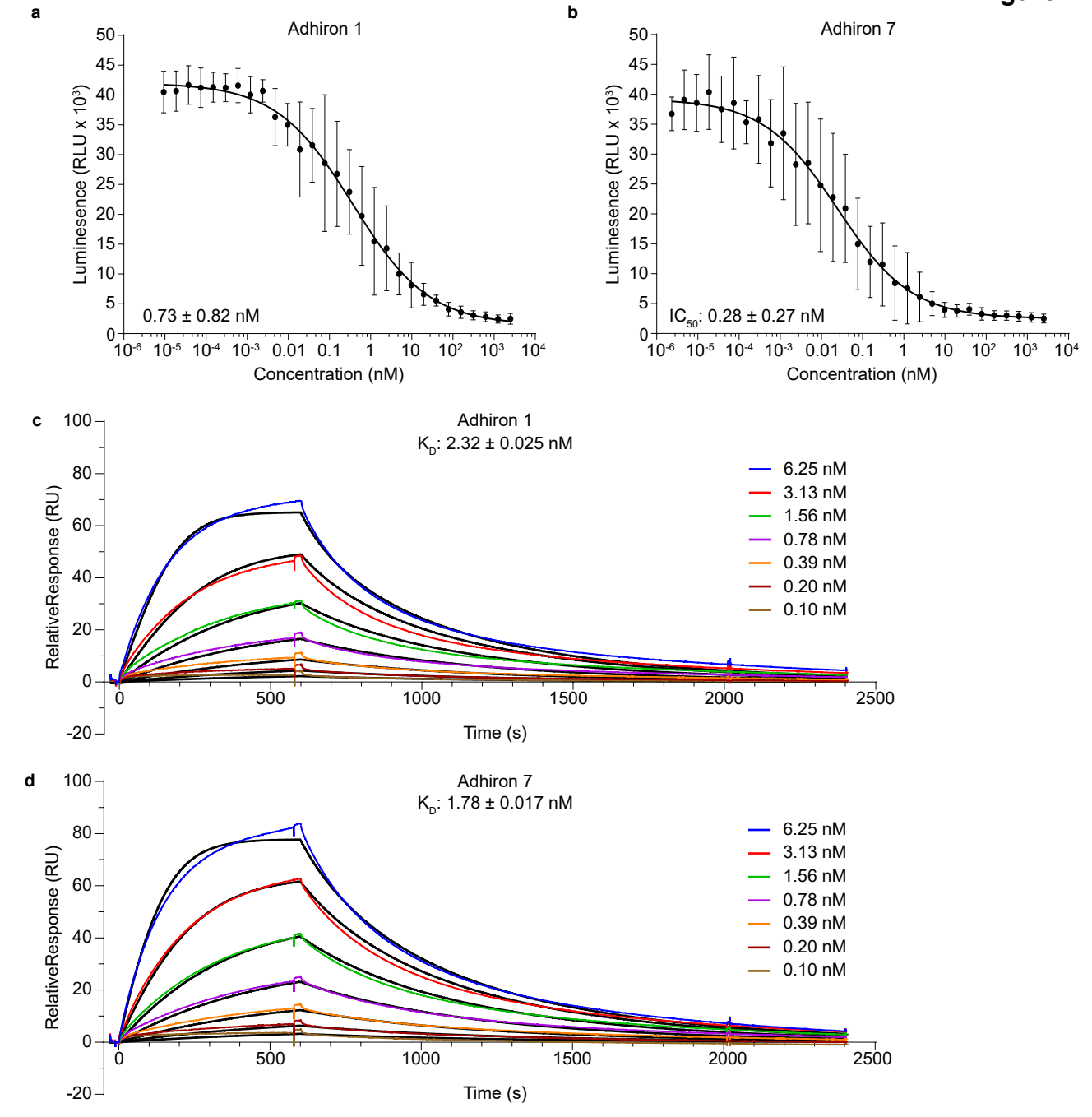
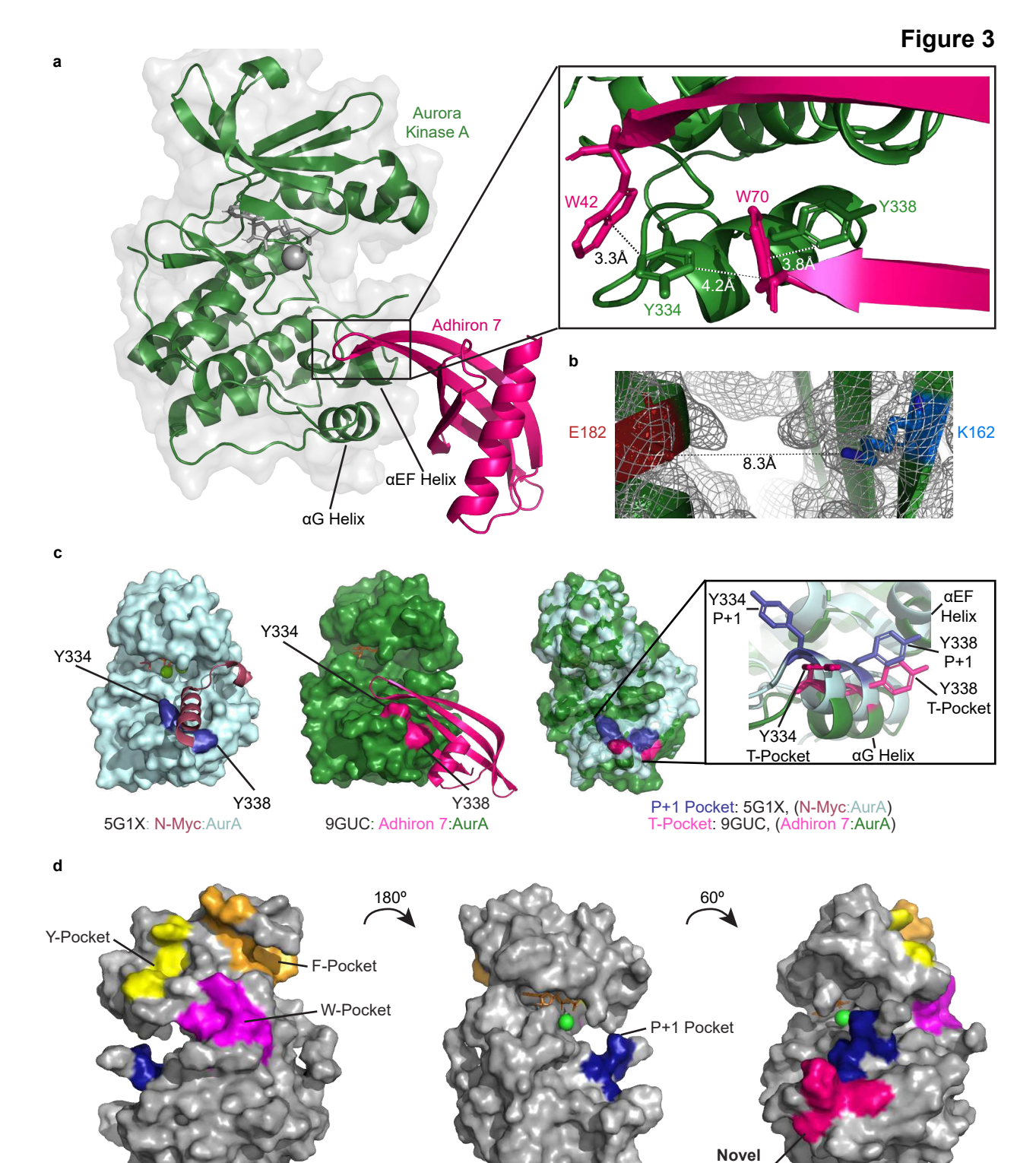


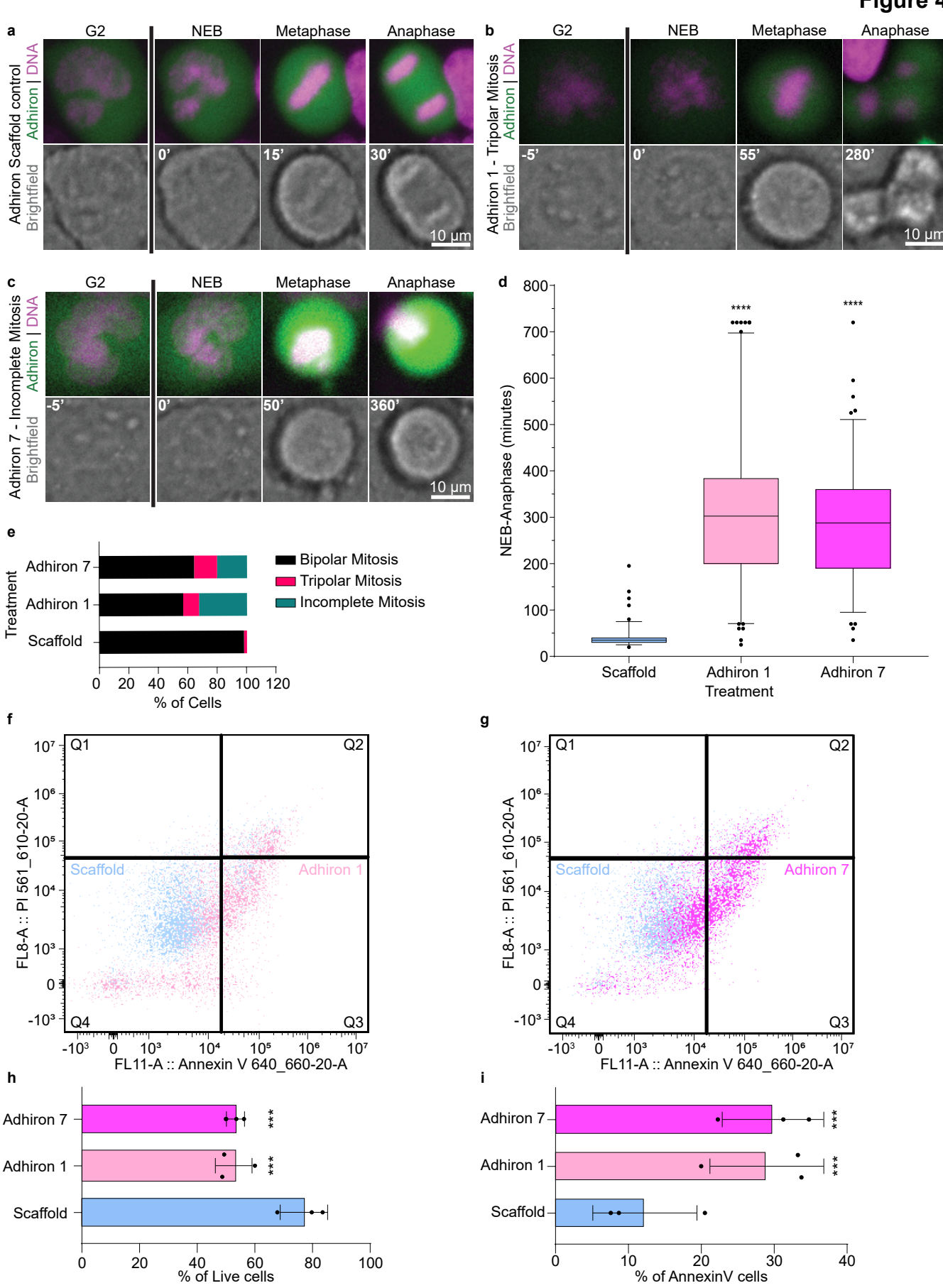
Figure 2





'T-Pocket'

Figure 4



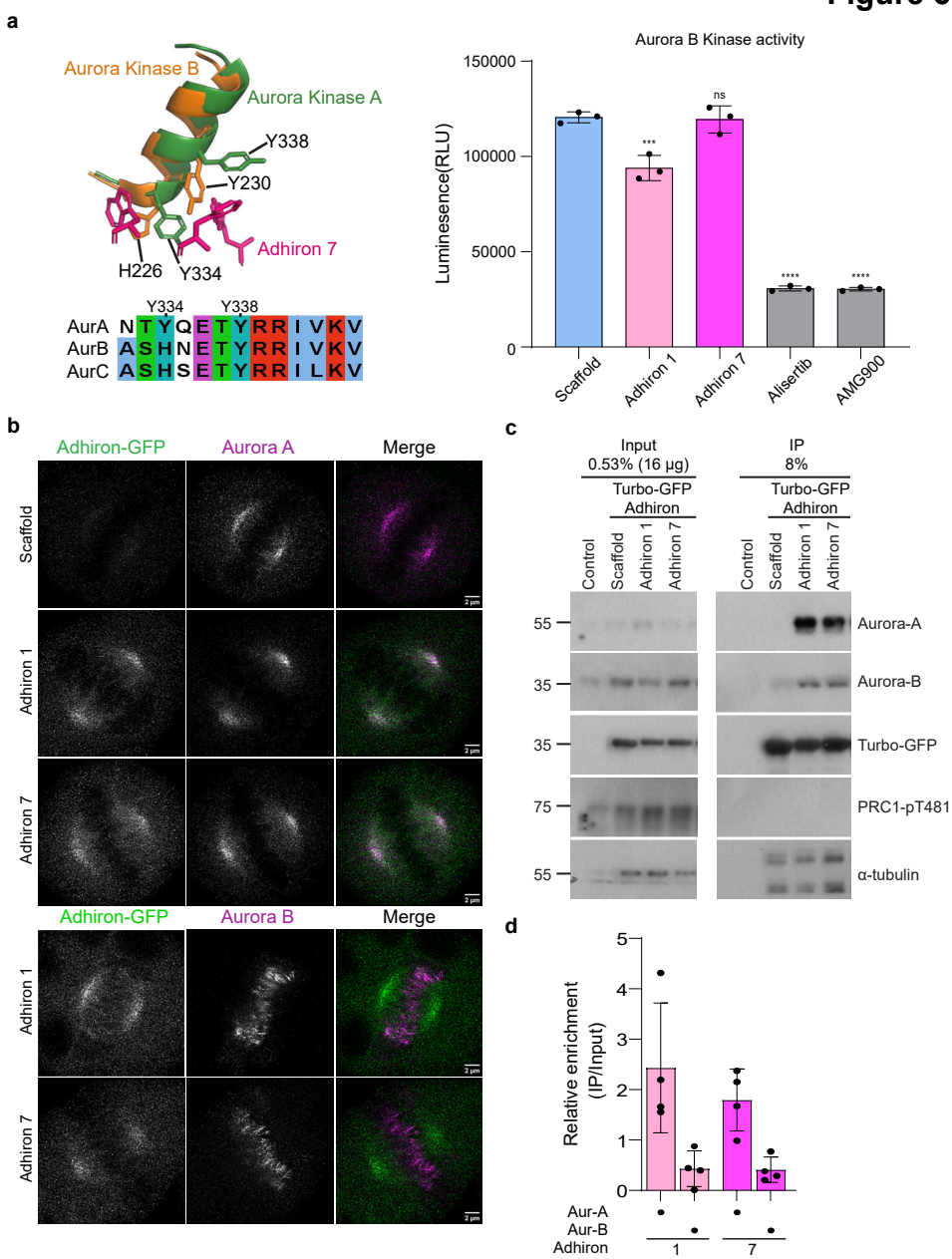
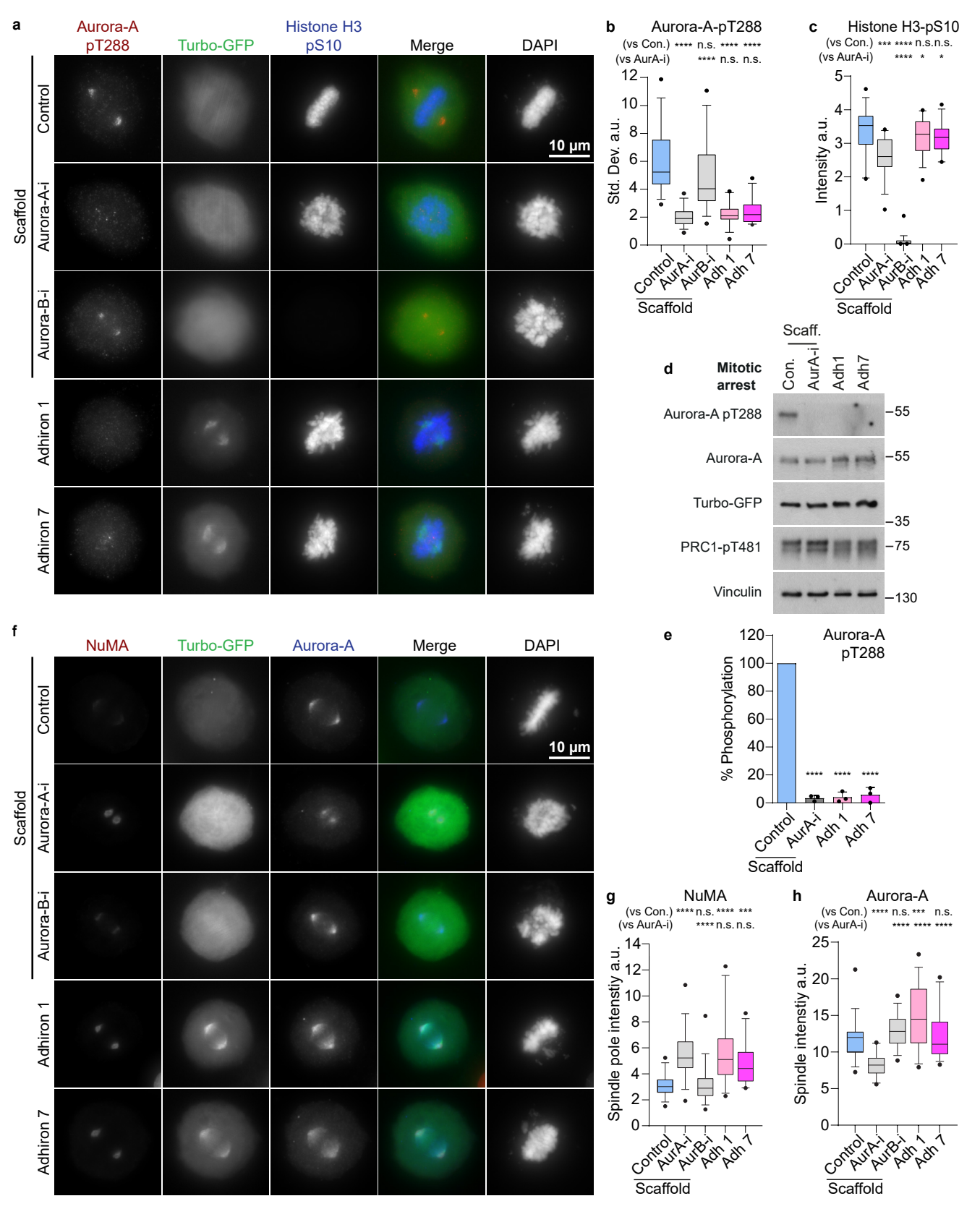
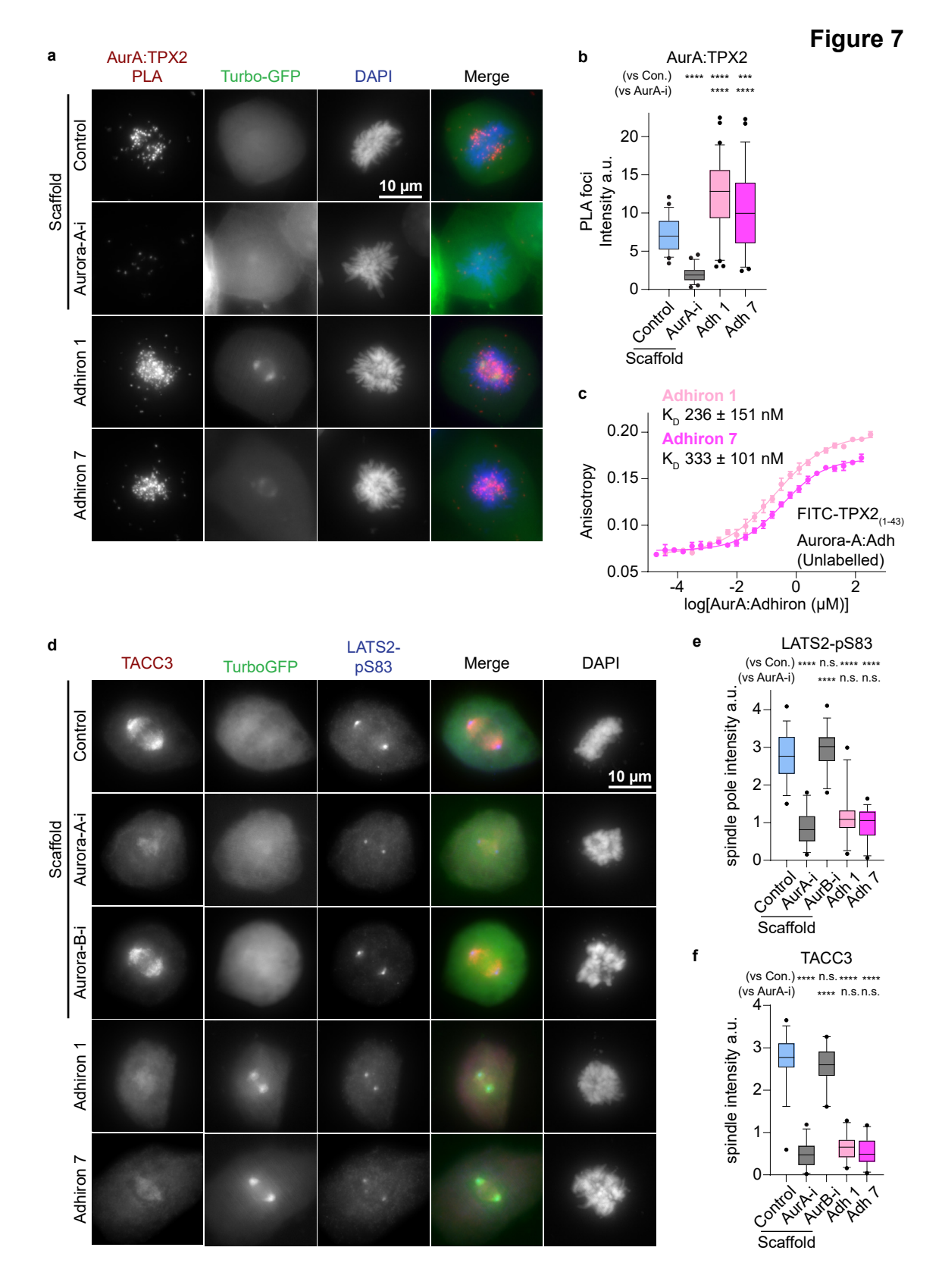
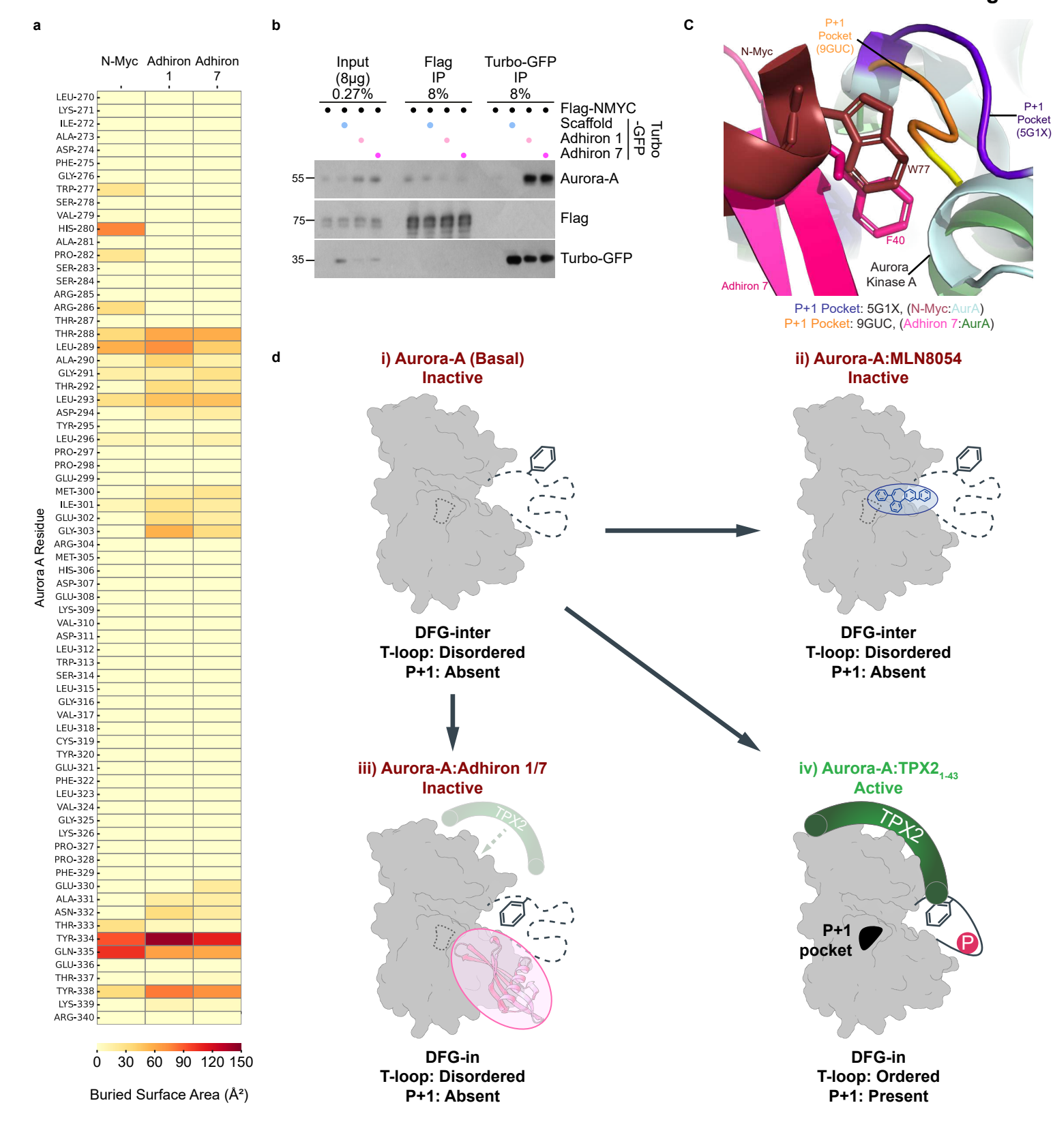


Figure 6







Supplementary Data: Synthetic protein binders reveal a cryptic regulatory pocket on Aurora A for selective allosteric inhibition

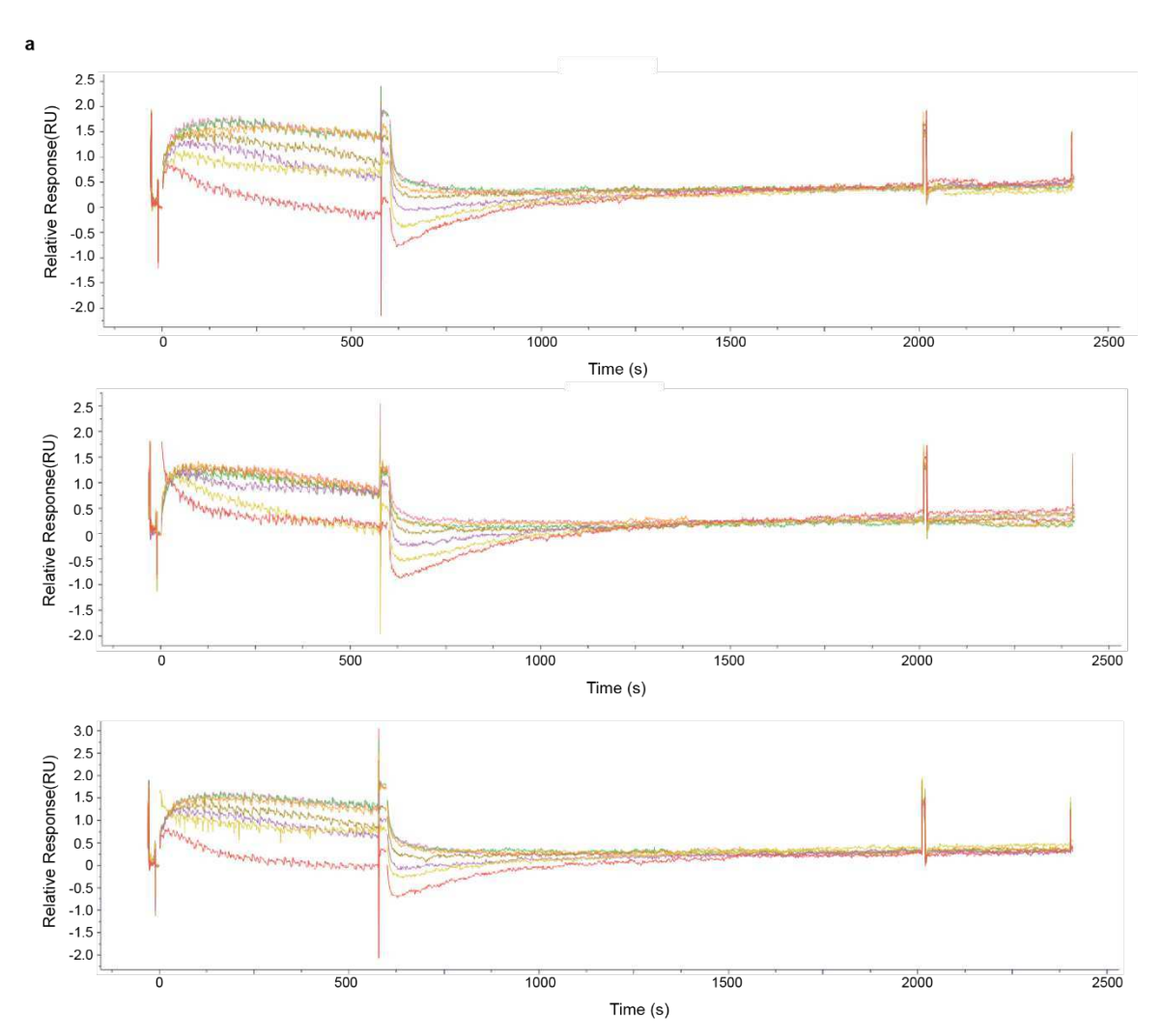


Figure 1 Sensorgrams of Scaffold control Adhiron.

a Scaffold Adhiron was immobilized on streptavidin-coated CM5 sensor chips via C-terminal biotin and differing concentrations of AurA⁽¹²²⁻⁴⁰³⁾ C290A, C393A were flowed over. Three separate repeats are shown, with raw data plotted and background subtracted.

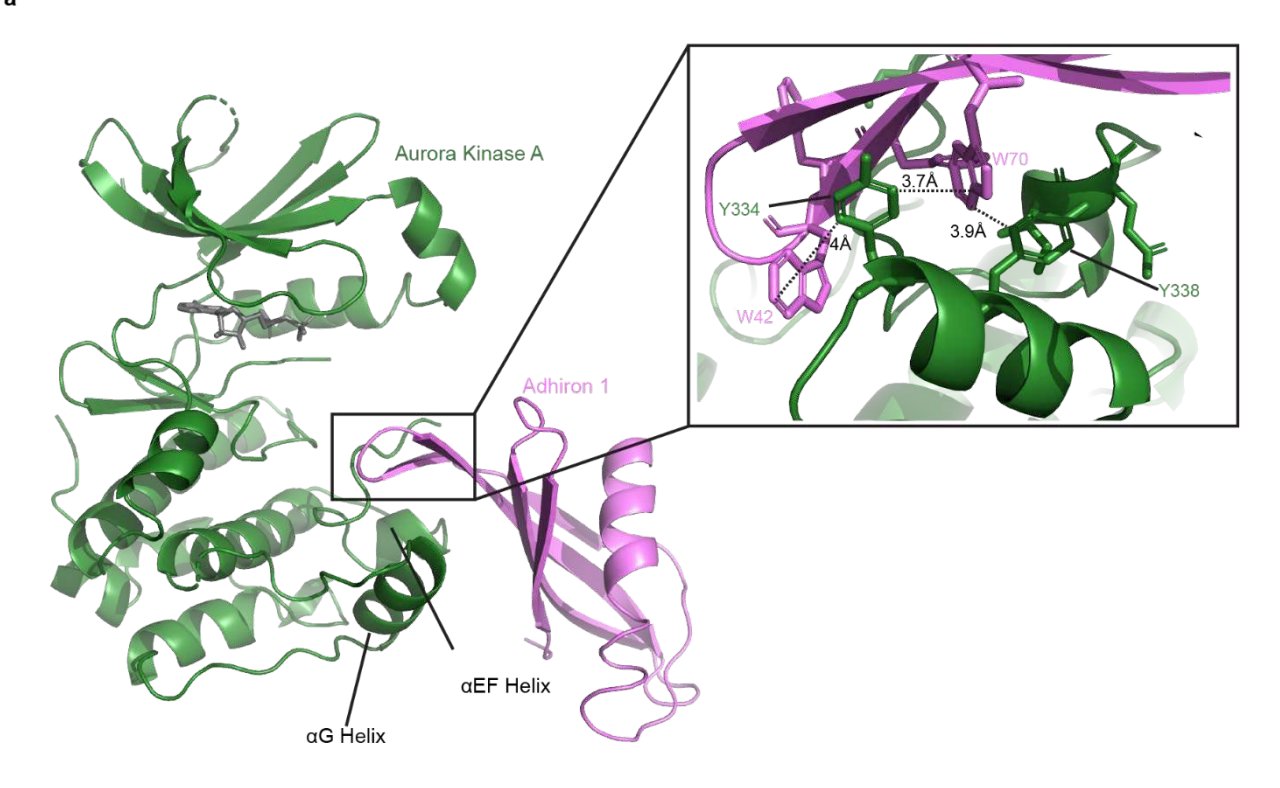


Figure 2 AurA:Adhiron 1 structure resolved to 2.4Å

a Crystal structure of the Aurora-AC290A/C393A 122-403 (AurA, green cartoon) in complex with Adhiron 1 residues (shown in powder-pink) with a magnified view of the structure with key residues shown as sticks.

Table 1 Data collection and refinement statistics (molecular replacement).

	AurA:Adhiron 7 (9GUC)	AurA:Adhiron 1 (9QVZ)
Data collection		
Space group	P 31 2 1 P 32 2 1	
Cell dimensions		
a, b, c (Å)	88.92, 88.92, 100.05	86.56, 86.56, 107.99
α, β, γ (°)	90.00, 90.00, 120.00	90.00, 90.00, 120.00
Resolution (Å)	40.66 – 2.10 (2.15-2.10) *	36 - 2.39 (2.43 - 2.39)
$R_{ m merge}$	0.0946 (0.7320)	0.036 (3.373)
Ι / σΙ	24.7 (5.4)	34.5 (0.8)
Completeness (%)	99.99 (97.60)	99.95 (99.70)
Redundancy	19.5 (14.5)	10.7 (10.5)
Refinement		
Resolution (Å)	2.10	2.39
No. reflections	27177	18994
R _{work} / R _{free}	0.1908 / 0.2319	0.2921 / 0.3358
No. atoms	5699	2603
Protein	5496	2533
Ligand/ion	108	70
Water	95	0
B-factors	43.00	97.79
Protein	42.48	97.45
Ligand/ion	69.01	110.24
Water	40.00	
R.m.s. deviations		
Bond lengths (Å)	0.0079	0.003
Bond angles (°)	1.74	0.63

Data for 9GUC and 9QVZ were collected from a single crystal of their respective complexes. *Values in parentheses are for highest-resolution shell.

Model	Activity	Spatial label	Dihedral label	C-helix-Salt Bridge
AurA:Adhiron1	Inactive	DFGin	Unassigned	out-out
AurA:Adhiron7	Inactive	DFGin	Unassigned	out-non

Figure 3 a Summary of KinCoRe analysis of Adhiron structures 1 and 7.

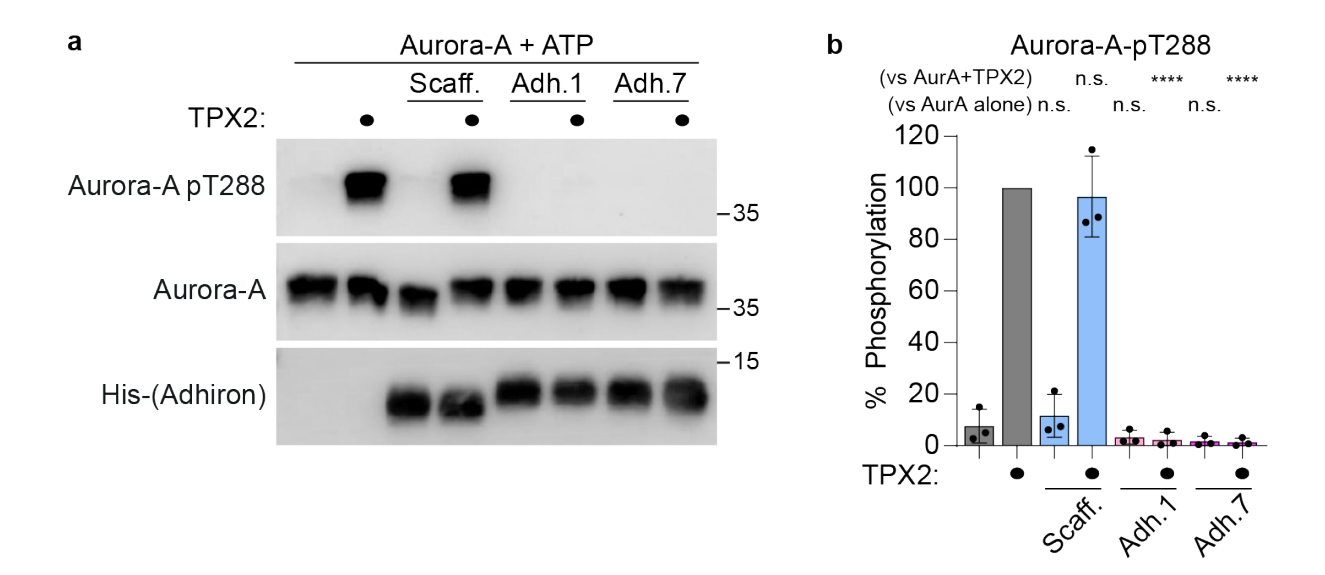


Figure 4 Adhiron modulation prevents AurA autophosphorylation.

a Western blot analysis of an Aurora-A autophosphorylation assay. Dephosphorylated Aurora A C290A/C393A (2 μ M) was incubated with ATP (160 μ M) and combinations of Adhiron Scaffold control, Adhirons 1 or 7 or TPX21-56, as indicated, all at 10-fold excess (20 μ M). Reactions were stopped after 90 minutes with SDS-PAGE loading buffer. **b** Densitometric quantification of Aurora-A-pT288 signal from **a**. Black bars indicate mean \pm S.D (n = 3 replicates). *p* values are denoted as follows: ****p < 0.0001, n.s not significant (one-way ANOVA).